Journal of Geochemical Exploration 166 (2016) 45–63

Contents lists available at ScienceDirect

Journal of Geochemical Exploration

journal homepage: www.elsevier.com/locate/gexplo

Trace element distribution in primary sulfides and Fe–Ti oxides from the sulfide-rich pods of the Lac des Iles Pd deposits, Western Ontario, Canada: Constraints on processes controlling the composition of the ore and the use of pentlandite compositions in exploration

C.J. Duran [a,*], S.-J. Barnes [a], J.T. Corkery [b,c]

[a] Université du Québec À Chicoutimi, Sciences de la Terre, 555 Blvd. de l'Université, Chicoutimi, QC G7H 2B1, Canada
[b] North American Palladium, Metals Exploration Division, 556 Tenth Ave., Thunder Bay, ON P7B 2R2, Canada
[c] Present address: TBay Explore Inc, 1100 Memorial Ave. Ste 376, Thunder Bay, ON P7B 4A3, Canada

ARTICLE INFO

Article history:
Received 8 October 2015
Revised 3 April 2016
Accepted 16 April 2016
Available online 20 April 2016

Keywords:
Lac des Iles Pd deposits
LA–ICP-MS
base-metal sulfides
Fe–Ti oxides
Mineral exploration

ABSTRACT

There is an on-going debate as to whether the Lac des Iles Pd deposits (Ontario, Canada) are of magmatic or hydrothermal origin. An aspect of the deposits that has not yet been documented is the presence of sulfide-rich pods which occur throughout the host intrusion (the Mine Block Intrusion). The ore mineralogy of the sulfide-rich pods consists of pyrrhotite, pentlandite, chalcopyrite, ± pyrite, magnetite and ilmenite. We present the trace element concentrations of pyrrhotite, pentlandite, chalcopyrite, magnetite, and ilmenite from the pods and compare these results with results from other Ni–Cu–platinum-group element (PGE) deposits. The low concentrations of Si and Ca and high concentrations of V, Ni, and Cr in magnetite are consistent with a magmatic origin of the magnetite. Variations in the V and Cr concentrations indicate that magnetite crystallized from a magmatic sulfide liquid during crystal fractionation of the sulfide liquid. The enrichments in Ni, Co, Os, Ir, Ru, and Rh and depletions in Cu, Ag, Cd, and Zn in pentlandite and pyrrhotite relative to chalcopyrite are also consistent with the formation of the pods by crystallization of a magmatic sulfide liquid. Comparison of pyrrhotite and pentlandite compositions from Lac des Iles with those from other Ni–Cu–PGE deposits shows that pyrrhotite and pentlandite derived from evolved magmas have distinct compositions relative to those derived from more primitive magmas. In addition, this comparison shows that pentlandites from PGE-dominated deposits are richer in Pd and Rh than pentlandites from Ni–Cu sulfide deposits. A plot of Pd vs Rh appears to be effective at distinguishing pentlandites of PGE-dominated deposits from those of Ni–Cu sulfide deposits and could possibly be used to adapt exploration strategies.

1. Introduction

The world-class Pd deposits of the Lac des Iles Complex, Western Ontario, Canada (referred to as the Roby, Offset, Twilight and High-grade zones) are hosted in varitextured meta-gabbronorites and chlorite-actinolite schists (Lavigne and Michaud, 2001; Barnes and Gomwe, 2011) and form wide zones (50–400 m) in which the mineralization occurs as disseminated base-metal sulfide (BMS) minerals and platinum-group minerals (PGM). These deposits are atypical in that they do not form thin stratiform layers (PGE-reef types) or massive to semi-massive sulfides at the margins of the intrusion and the ore has very high Pd/Ir and Pd/Pt ratios. Furthermore, the Lac des Iles Pd deposits have undergone alteration that could have affected the initial composition of the ore (Hinchey and Hattori, 2005; Somarin et al., 2009; Barnes and Gomwe, 2011; Hanley and Gladney, 2011; Djon and Barnes, 2012; Boudreau et al., 2014), particularly in the High-grade Zone, which consists of chlorite–actinolite schists. This has led to a debate as to whether the sulfide minerals crystallized from magmatic sulfide liquids and were subsequently altered (Hinchey et al., 2005; Barnes and Gomwe, 2011; Djon and Barnes, 2012) or whether they crystallized directly from aqueous magmatic fluids that percolated through the magma pile (Boudreau et al., 2014; Schisa et al., 2015).

In addition to the disseminated mineralization, sulfide-rich pods have been identified throughout the intrusion (Duran et al., 2016). Duran et al. (2016) interpret the sulfide-rich pods as cumulates of monosulfide solid solution (MSS) and the disseminated sulfides as the product of in situ crystallization of a sulfide liquid. A similar relationship between disseminated and sulfide-rich mineralization has also been proposed for some Ni–Cu sulfide deposits such as Aguablanca in Spain (Piña et al., 2008) and Jinchuan in China (Chen et al., 2014).

Since the advent of laser ablation inductively coupled plasma mass spectrometry (LA–ICP-MS), the chalcophile and platinum-group element (PGE) geochemistry of BMS has been investigated in a variety of

* Corresponding author.
E-mail address: charley.duran@hotmail.fr (C.J. Duran).

http://dx.doi.org/10.1016/j.gexplo.2016.04.005
0375-6742/

PGE reefs and Ni–Cu sulfide deposits (e.g., Huminicki et al., 2005; Barnes et al., 2006, 2008; Holwell and McDonald, 2007; Godel et al., 2007, 2012; Godel and Barnes, 2008; Hutchinson and McDonald, 2008; Dare et al., 2010, 2011, 2014a; Piña et al., 2012; Osbahr et al., 2013, 2014; Smith et al., 2014; Chen et al., 2014), including the disseminated mineralization of Lac des Iles (Djon and Barnes, 2012). The approach in these studies was to assess the influence of crystal fractionation of sulfide liquids on the distribution of the elements among the BMS. Owing to the presence of secondary accessory minerals (e.g., pyrite and millerite) in some deposits this approach has also been useful for highlighting the redistribution of some elements during post-magmatic processes (Djon and Barnes, 2012; Piña et al., 2013; Smith et al., 2014). In addition, the geochemistry of magnetite has been used as an indicator of provenance and petrogenesis (Dare et al., 2012, 2014b; Nadoll et al., 2014; Boutroy et al., 2014) as the magnetite records the composition of the magmatic liquid/hydrothermal fluid from which it crystallizes.

Sulfide-rich pods from Lac des Iles exhibit the typical mineral assemblage observed in magmatic Ni–Cu–PGE deposits (i.e., pyrrhotite, pentlandite chalcopyrite and minor magnetite). In addition, pyrite is present in many pods. This pyrite has been attributed to post-cumulus alteration of the pods by Duran et al. (2015) and is not the topic of the current study. Here we present the trace element concentrations of pyrrhotite, pentlandite, chalcopyrite, and Fe–Ti oxides (magnetite and ilmenite) using LA–ICP-MS and compare them with studies from other Ni–Cu–PGE deposits. The first objective of this study was to address whether the primary ore-mineral assemblage originated from magmatic sulfide liquid. The second objective was to consider the implications of the growing data base of trace elements for these minerals for petrogenesis and mineral exploration.

2. Analytical method

Details of sample selection are presented in Duran et al. (2016). Pyrrhotite, pentlandite, chalcopyrite, magnetite and ilmenite were identified and described using an OLYMPUS DP71 optical microscope at Université du Québec à Chicoutimi (UQAC). Petrographic investigation was carried out on 74 polished thin sections and 12 polished blocks made from 43 sulfide-rich samples. A total of 15 representative sulfide-rich samples were selected and used to determine in situ composition of BMS, Fe–Ti oxides, or both.

LA–ICP-MS analysis was performed at LabMaTer (UQAC) using an Excimer 193 nm Resonetics Resolution M-50 laser ablation system coupled with an Agilent 7700× mass spectrometer. A range of beam sizes from 43 to 75 μm, a range of stage movement speeds from 2.5 to 5 μm/s, a range of laser frequencies from 10 to 15 Hz and a range of power from 4 to 5 mJ/pulse were used to analyze the minerals. For large grains a traverse across the grain was made, and for small grains spot analyses were performed. The gas blank was measured for 30 s before switching on the laser for at least 60 s. The ablated material was carried into the ICP-MS by an argon–helium gas mix at a rate of 0.8–1 L/min for Ar and 350 mL/min for He. Data reduction was carried out using the Iolite package for Igor Pro software (Paton et al., 2011). Internal standardization was based on ^{57}Fe using the stoichiometric iron values of each mineral species.

Details of the analytical method for the sulfide minerals are given in Duran et al. (2015). For sulfide signals containing silicate, oxide, or PGM inclusions, the sulfide-only intervals were selected for data reduction in order to have pure sulfide compositions. For oxides, counts of the following isotopes were monitored: ^{25}Mg, ^{27}Al, ^{29}Si, ^{34}S, ^{44}Ca, ^{45}Sc, ^{47}Ti, ^{49}Ti, ^{51}V, ^{52}Cr, ^{53}Cr, ^{55}Mn, ^{57}Fe, ^{59}Co, ^{60}Ni, ^{63}Cu, ^{65}Cu, ^{66}Zn, ^{69}Ga, ^{71}Ga, ^{74}Ge ^{75}As, ^{89}Y, ^{90}Zr, ^{92}Zr, ^{93}Nb, ^{95}Mo, ^{107}Ag, ^{111}Cd, ^{118}Sn, ^{121}Sb, ^{178}Hf, ^{181}Ta, ^{182}W, and ^{208}Pb. Silicon and sulfur were monitored to ensure that the measured signal represented pure oxide. For signals containing Si or S, the oxide-only intervals were selected for data reduction. Three certified reference materials were used for external calibration of the LA–ICP-MS data: GSE-1g, which is a synthetic glass supplied by the United States Geological Survey (USGS), was used to calibrate for all elements; GSD-1g, which is also a synthetic glass supplied by the USGS, and BC28, which is a natural magnetite from the Main Magnet Seam of the Bushveld Complex, were both used as in-house reference materials to monitor the calibration of GSE-1g. According to Dare et al. (2012), interferences of ^{90}Zr with ^{50}Ti^{40}Ar, ^{50}V^{40}Ar and ^{50}Cr^{40}Ar; ^{92}Zr with ^{52}Cr^{40}Ar; and ^{93}Nb with ^{53}Cr^{40}Ar are negligible, thus corrections were not required. The results of the monitors for both sulfides and oxides were generally within 10% analytical error of the working values and relative standard deviation (RSD) was typically at <10%. The results of the monitors for both sulfides and oxides are presented in the electronic supplementary material.

3. Geological background

An overall description of the geology of the Lac des Iles Complex, including the Pd mine and deposits, has been presented in Hinchey et al. (2005) and Barnes and Gomwe (2011) and only a brief overview is presented here. The complex is located in Western Ontario, approximately 80 km north of Thunder Bay, near the boundary between the Wabigoon and Quetico subprovinces of the Superior province. The Lac des Iles Complex (2689 ± 1 Ma: Stone et al., 2003) forms a suite of mafic to ultramafic intrusions emplaced in granitoids. The Pd mine and deposits occur within the central intrusion of the complex, the Mine Block Intrusion (Fig. 1).

At the surface, the Mine Block Intrusion appears to be oval in plan view and funnel-shaped in profile (Fig. 1). The intrusion is elongated along a SW–NE trend similar to regional faults (Gupta and Sutcliffe, 1990), and is affected by many syn- and post-magmatic shear zones and faults. These structures have been related to a continual deformation history while the Mine Block Intrusion was emplaced (Rankin, 2013).

The different lithological units of the Mine Block Intrusion display a radial stratigraphy, which suggests that the intrusion crystallized inwards (Schisa et al., 2015). The rocks mainly consist of noritic to gabbronoritic adcumulates with extremely variable textures (e.g., magmatic breccias, varitextured and pegmatitic rocks). Most of the rocks are altered to greenschist and lower amphibolite facies (Boudreau et al., 2014). Adcumulate textures were considerably altered to form a secondary mineral assemblage. Plagioclase was variably altered to form sericite, epidote-group minerals, chlorite, and carbonates. Orthopyroxene was more significantly altered to form actinolite and chlorite, being locally completely replaced (Barnes and Gomwe, 2011; Boudreau et al., 2014).

Based on the orthopyroxene and plagioclase trace element contents of fresh rocks from the ore zones, Barnes and Gomwe (2010) estimated the composition of the initial silicate liquid at the time of the formation of the ore. The composition of this calculated liquid appears to be similar to arc andesites. This interpretation is consistent with the model of Brügmann et al. (1997), in which it is suggested that the tectonic setting for the emplacement of the Lac des Iles Complex was the root of a continental arc. In contrast, Hinchey et al. (2005) suggested that the magma that formed the ores was similar to enriched mid oceanic ridge basalts (E-MORB), which would require an ocean island or seamount setting.

The main zone of mineralization (i.e., Roby Zone) occurs in the western part of the Mine Block Intrusion (Fig. 1). The surface exposure consisted of varitextured metagabbronorites interpreted as magmatic breccias, which contain approximately 1 modal percent of BMS (e.g., Lavigne and Michaud, 2001; Hinchey et al., 2005; Barnes and Gomwe, 2011). On the eastern edge of the Roby Zone there is a 15–30 m wide sheared unit composed of chlorite–actinolite schists and known as the High-grade Zone. The Roby Zone extends to the depth at which it is cut by the Offset Fault. Below the Offset Fault, the mineralization is displaced approximately 250 m to the west of the overlying Roby Zone and is known as the Offset Zone (Fig. 1). Other areas of

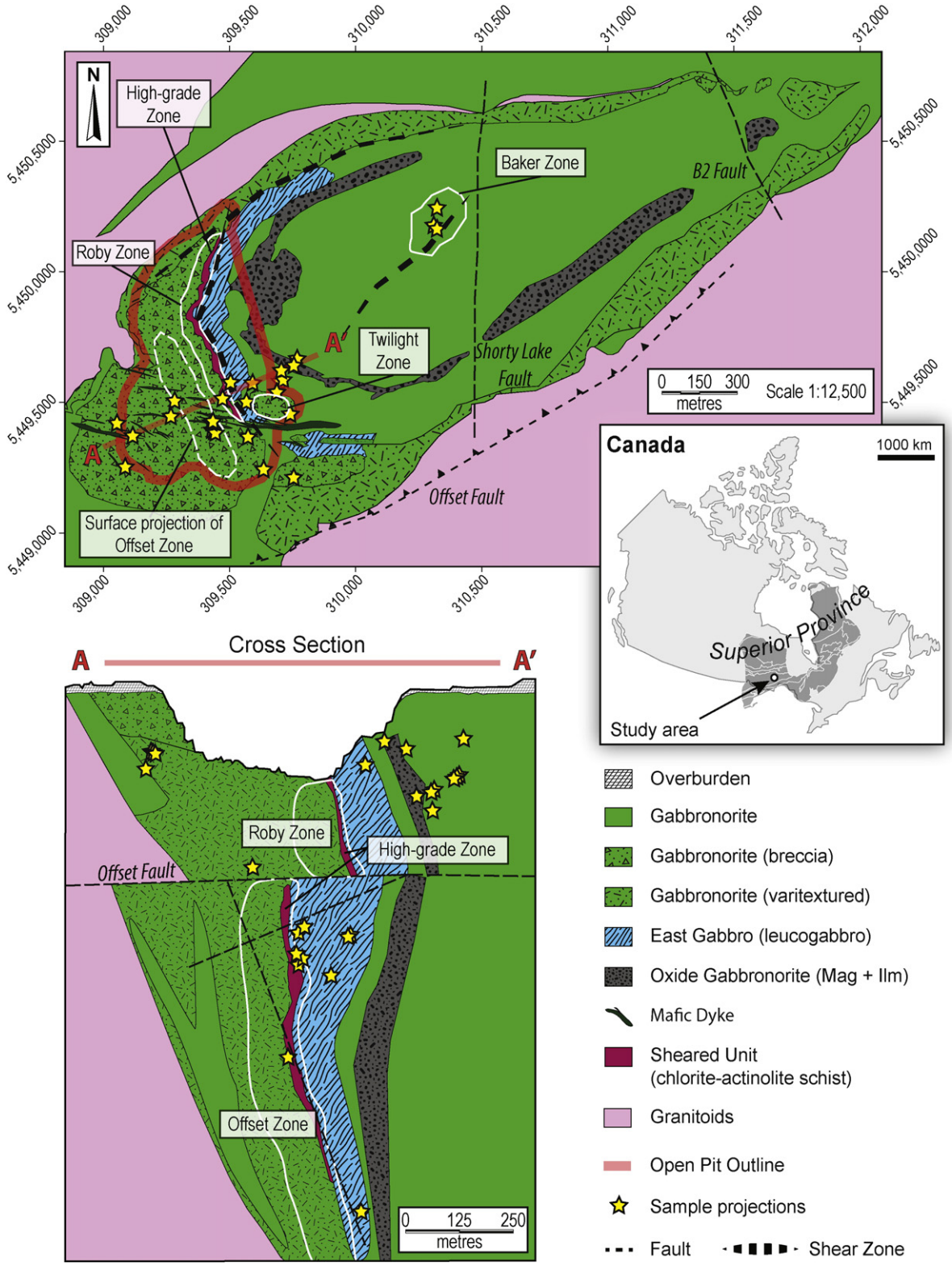

Fig. 1. Simplified geological map and idealized cross section of the Mine Block Intrusion of the Lac des Iles Complex with projected locations of sulfide-rich samples (modified from North American Palladium). Note that sulfide-rich samples follow a SW–NE orientation. Sulfides-rich pods sampled from the open pit and from the Baker Zone are not plotted on the cross-section. The ore zones are outlined in white, except the High-grade Zone that corresponds to the sheared unit.

mineralization are present within the Mine Block Intrusion (e.g., Baker Zone: Fig. 1) but are not currently mined.

In addition to the disseminated mineralization, sulfide-rich pods are present throughout the intrusion. These sulfide-rich pods occur throughout the stratigraphy, in all rock types and along syn-magmatic shear zones (Fig. 1). Although their host rocks have been altered to greenschist and lower amphibolite facies, as have been most of the rocks in the intrusion, no alteration halos have been observed proximal to the pods. These pods contain net-textured to massive sulfides, in which enclosed silicate minerals are randomly oriented. No evidence

of ductile deformation and/or recrystallization has been identified in the sulfide minerals but silicate minerals surrounding the pods show evidence of high-temperature deformation (Duran et al., 2016). On this basis Duran et al. (2016) suggested that, due to high-temperature deformation, gashes opened in the cumulus magma pile while it was not completely consolidated and magmatic sulfide liquids migrated into these dilation zones to form the sulfide-rich pods.

4. Petrography of sulfide-rich pods

The sulfide-mineral assemblage of the sulfide-rich pods from Lac des Iles consists of pyrrhotite, pentlandite, pyrite, and chalcopyrite. The amount of pyrite within the pods is extremely variable, with pyrite ranging from being nearly absent to being the predominant sulfide mineral. Duran et al. (2015) showed that pyrite formed by a process of post-cumulus re-equilibration of the ore and petrographic details on pyrite are presented in this study. Pyrrhotite forms large anhedral grains and is associated with pentlandite (Fig. 2a, b). Pentlandite occurs in three forms: as coarse polycrystalline aggregates, chain-like veinlets around pyrrhotite, and oriented exsolution flames within pyrrhotite (Fig. 2a-c). This textural relationship is commonly observed in magmatic Ni–Cu–PGE deposits (e.g., Dare et al., 2010) and experiments demonstrated that it results from the exsolution of pyrrhotite and pentlandite from MSS (e.g., Kelly and Vaughan, 1983). Typically, the pyrrhotite–pentlandite assemblage is associated with minor anhedral grains of chalcopyrite that are randomly dispersed between pyrrhotite and pentlandite grains (Fig. 2c). At the margins of a few pods, chalcopyrite is the predominant sulfide mineral. Description of this occasional chalcopyrite-rich assemblage and its relation to the pyrrhotite–pentlandite-rich assemblage are presented in Duran et al. (2016).

In addition to sulfide minerals, Fe–Ti oxides (i.e., magnetite and ilmenite) are present in the sulfide-rich pods. In most samples, the magnetite and ilmenite form small anhedral grains scattered within pyrrhotite grains or at sulfide–silicate grain interfaces (Fig. 2d, e). Ilmenite occasionally contains micron-sized hematite exsolutions (Fig. 2e). In some cases, the magnetite has been observed to form large anhedral patches (Fig. 2f) that are associated with large anhedral grains of pyrrhotite and silicate minerals.

5. Results and discussion

The first phase to crystallize from a magmatic sulfide liquid is MSS (Naldrett et al., 1967). Iron oxide starts to crystallize next (Naldrett, 1969), and intermediate solid solution (ISS) crystallizes last (Cabri,

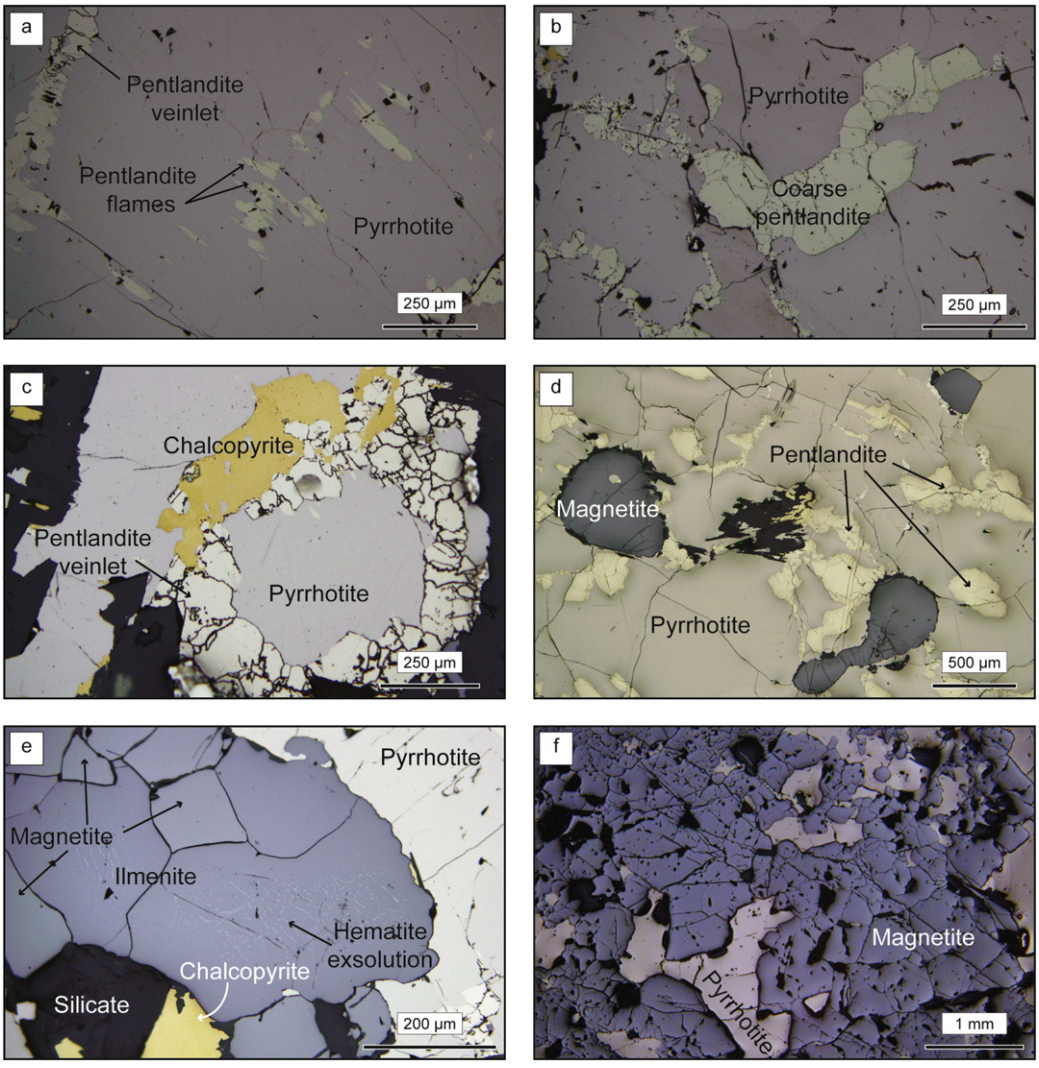

Fig. 2. Photomicrographs in reflected light of the primary base-metal sulfides and Fe–Ti oxides observed in the sulfide-rich pods; (a) pyrrhotite with oriented pentlandite exsolution flames; (b) pyrrhotite with coarse pentlandite; (c) pyrrhotite, pentlandite and chalcopyrite. Pentlandite forms a polycrystalline veinlet around the pyrrhotite; (d) pyrrhotite–pentlandite assemblage with small rounded anhedral magnetite; (e) magnetite and ilmenite at the sulfide/silicate interface. Note that hematite exsolutions are present within ilmenite; (f) large patch of magnetite with pyrrhotite.

1973). As the temperature decreases, all three phases undergo exsolution. Monosulfide solid solution exsolves to form pyrrhotite and pentlandite ± minor pyrite (Kelly and Vaughan, 1983). Iron oxide exsolves to form magnetite ± ilmenite (Buddington and Lindsley, 1964) and ISS exsolves to form chalcopyrite ± pentlandite (Dutrizac, 1976). To assess whether sulfide and oxide minerals from the Lac des Iles sulfide-rich pods followed this crystallization sequence, we investigated their composition and trace element distribution. Then we compared our results with those of well-characterized Ni–Cu–PGE deposits to consider the influence of various processes such as the degree of fractionation of the parental magma from which sulfide liquids segregated, timing of oxide crystallization, exsolution of MSS, and deformation. Finally, we discuss the implications for mineral exploration.

5.1. Sulfide compositions

The median composition of each BMS is presented in Table 1, along with the minimum and maximum values. The full data set is presented in the electronic supplementary material. Within the BMS, most elements are homogeneously distributed as indicated by the time–signal diagrams (Fig. 3). Thus, median compositions are considered to be representative for most elements. Silver, Bi, and Pb are exceptions to this in most pentlandite and in some pyrrhotite and they show irregular distributions (Fig. 3b, d). Additionally, Re–Mo bearing inclusions have been intersected in some pyrrhotite grains.

The compositions of BMS are traditionally plotted on primitive mantle normalized patterns of PGE and a limited number of other metals to investigate the processes that control the PGE distribution (e.g., Barnes et al., 2006; Chen et al., 2014). Because of advancements in the capabilities of LA–ICP-MS, a wider range of elements may now be considered. To incorporate these elements, we propose a new multi-element diagram for sulfides. This diagram is designed to emphasize the partitioning behavior of trace elements during crystal fractionation of sulfides. Therefore, we plot the elements from left to right in decreasing order of compatibility in the first phase crystallizing from magmatic sulfide liquids, MSS. However, to preserve the shape of the PGE patterns, the PGE have been kept together, in order of increasing melting point (and are therefore not positioned in order of compatibility in MSS).

Each BMS mineral has its own distinctive normalized trace element pattern, as can be seen from Fig. 4. To test whether the variation in the geochemistry is controlled by MSS crystal fractionation, we may assess the distribution of the elements among the BMS with respect to their compatibility in MSS, proceeding from the left hand side of the diagram to the right. For instance, the partition coefficient for Se into MSS is slightly less than 1, and slightly more than 1 into ISS (Helmy et al., 2010; Liu and Brenan, 2015). Thus, Se is expected to concentrate in similar proportions in pyrrhotite, pentlandite, and chalcopyrite. All three BMS have Se concentrations of approximately 100 ppm, and plot on the same level on the diagram (Fig. 4).

Rhenium and Mo concentrations are slightly higher in pyrrhotite (from ≤0.006 to 0.324 and from 0.108 to 0.297 ppm, respectively) and pentlandite (from ≤0.006 to 25.7 and from 0.039 to 2.96 ppm, respectively) than in chalcopyrite (from ≤0.006 to 0.286 and from 0.052 to 0.660 ppm, respectively). These elements have similar levels on the BMS patterns (Fig. 4). However, Re and Mo are not compatible in ISS and are expected to concentrate in MSS (Brenan, 2008; calculated from Li and Audétat, 2012; Liu and Brenan, 2015). The low abundance of these elements in pyrrhotite and pentlandite and the lack of correlations with other compatible elements may reflect the presence of Re–Mo bearing minerals (Fig 3e). The presence of Re and Mo in solid solution within pyrrhotite and pentlandite and as inclusions within pyrrhotite grains, suggests to us that Re and Mo were initially concentrated into MSS prior to their exsolution as distinct minerals. A similar interpretation has been proposed by Godel and Barnes (2008) and Dare et al. (2010) for the Stillwater Complex and Sudbury, respectively.

Cobalt and Ni display different behavior on the three BMS patterns (Fig. 4). Pentlandite has Co and Ni concentrations that are approximately 100 times those of the primitive mantle. Pyrrhotite has intermediate values that are 2 to 4 times those of the primitive mantle. Chalcopyrite has a Co concentration that is approximately 0.005 times that of the primitive mantle. At high temperature, Co and Ni are slightly incompatible in MSS, but upon cooling, they become compatible and partition into MSS (Li et al., 1996; Mungall et al., 2005). The higher concentrations of these elements in pentlandite and pyrrhotite relative to chalcopyrite (Fig. 4) reflect their partitioning into MSS during crystal fractionation. This type of correlation can be readily noticed on a plot of Co versus Ni (Fig. 5), in which pyrrhotite and pentlandite exhibit a positive correlation,

Table 1
Compositions of base-metal sulfides from Lac des Iles sulfide-rich pods as determined by LA–ICP-MS analysis.

Element		Isotope	Pyrrhotite			Pentlandite			Chalcopyrite		
			n = 37			n = 55			n = 20		
			Median	Min	Max	Median	Min	Max	Median	Min	Max
Co	(ppm)	^{59}Co	156	21.7	353	6720	137	16,736	5.52	0.279	5538
Ni	(ppm)	^{61}Ni	7099	3048	10,671	246,805	192,104	280,342	2042	420	22,823
Cu	(ppm)	^{65}Cu	0.262	0.061	636	1.42	0.326	4689	345,381	253,482	351,162
As	(ppm)	^{75}As	0.773	≤0.455	2.05	0.762	≤0.455	7.91	0.771	≤0.455	8.12
Se	(ppm)	^{82}Se	125	65.4	341	79.1	37.6	1931	153	42.7	239
Mo	(ppm)	^{95}Mo	0.181	0.108	0.297	0.086	0.039	2.96	0.099	0.052	0.660
Ru	(ppm)	^{101}Ru*	0.026	≤0.017	0.303	0.080	≤0.017	0.679	0.125	0.018	0.260
Rh	(ppm)	^{103}Rh*	0.014	≤0.003	0.095	0.058	0.013	1.41	n.a.	n.a.	n.a.
Pd	(ppm)	^{108}Pd*	0.025	≤0.010	0.307	18.3	0.401	785	1.26	0.033	141
Ag	(ppm)	^{109}Ag	0.335	0.139	1.16	2.60	0.208	70.3	33.6	1.126	83.3
Cd	(ppm)	^{111}Cd	≤0.054	≤0.054	0.374	≤0.054	≤0.054	2.21	0.843	0.067	7.36
Sn	(ppm)	^{118}Sn	0.126	0.069	56.1	0.080	≤0.032	22.5	0.152	≤0.032	1.64
Sb	(ppm)	^{121}Sb	0.025	≤0.012	0.056	0.016	≤0.012	0.326	0.017	≤0.012	0.049
Te	(ppm)	^{128}Te	0.299	≤0.194	0.841	0.287	≤0.194	5.14	0.262	≤0.194	4.84
Re	(ppm)	^{185}Re	0.016	≤0.006	0.324	0.012	≤0.006	25.7	0.009	≤0.006	0.286
Os	(ppm)	^{189}Os	0.023	≤0.016	0.175	≤0.016	≤0.016	0.414	≤0.016	≤0.016	0.049
Ir	(ppm)	^{193}Ir	0.016	≤0.004	0.070	0.009	≤0.004	0.029	≤0.004	≤0.004	0.027
Pt	(ppm)	^{195}Pt	≤0.014	≤0.014	0.056	0.015	≤0.014	0.485	≤0.014	≤0.014	0.520
Au	(ppm)	^{197}Au	0.011	≤0.008	0.050	0.012	≤0.008	0.133	0.012	≤0.008	0.075
Pb	(ppm)	^{208}Pb	0.430	0.075	6.79	2.62	0.083	234	3.38	1.50	42.0
Bi	(ppm)	^{209}Bi	0.050	0.004	1.47	0.088	≤0.003	2.784	0.117	0.010	4.72

n = number of analysis; min = minimum value; max = maximum value; * = values corrected for interference; n.a. = not available (for chalcopyrite the interference of ^{103}Rh with ^{63}Cu^{40}Ar made it impossible to accurately determine the Rh concentrations).

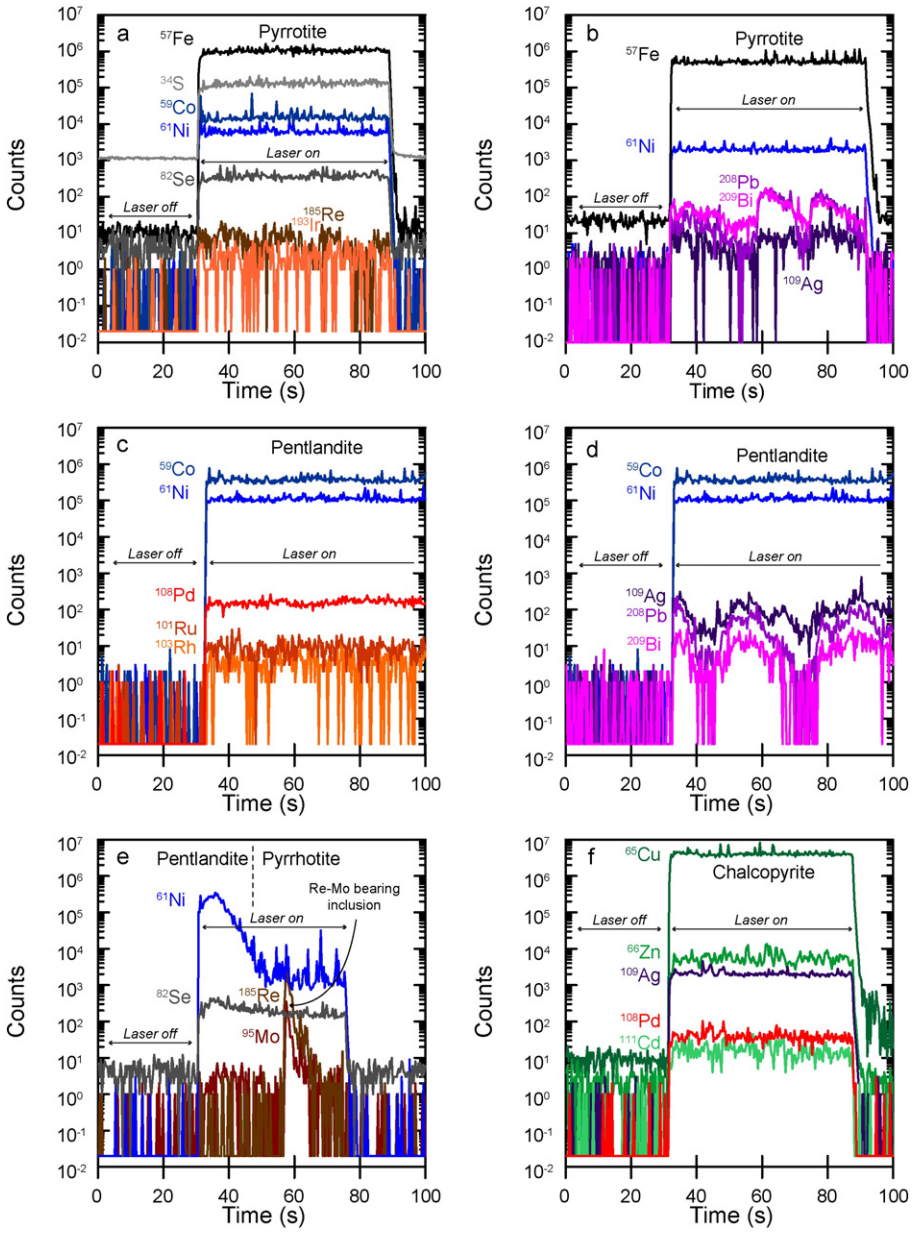

Fig. 3. Examples of time–signal diagrams for base-metal sulfides; (a–b) pyrrhotite; (c–d) pentlandite; (e) pyrrhotie + pentlandite with Re–Mo bearing inclusion; (f) chalcopyrite.

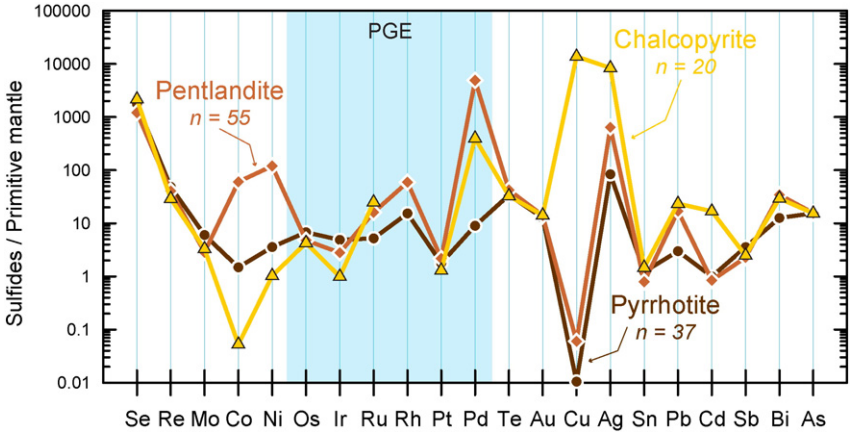

Fig. 4. Primitive mantle normalized multi-element diagram of pyrrhotite, pentlandite, and chalcopyrite from Lac des Iles sulfide-rich pods. The normalization values are from Lyubetskaya and Korenaga (2007).

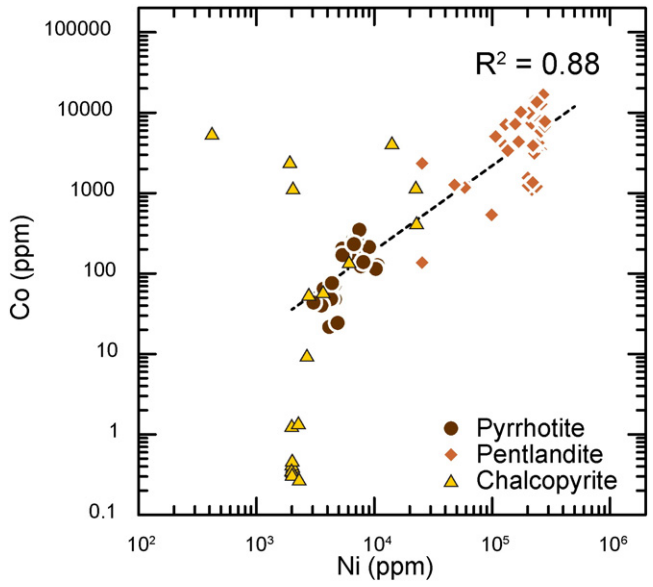

Fig. 5. Binary diagram of Co versus Ni. Note the high degree of correlation for pyrrhotite and pentlandite.

whereas chalcopyrite does not. Furthermore, Co and Ni are preferentially concentrated in pentlandite with values of up to 16,736 ppm for Co. This result reflects the preference of these elements for pentlandite over pyrrhotite during exsolution of MSS.

As in the case of Ni and Co, IPGE (Os, Ir, and Ru) and Rh are compatible in MSS. Pyrrhotite displays a relatively flat pattern from Os to Ru, with a slight increase toward Rh, and pentlandite displays a strong increase from Ir to Rh (Fig. 4). In contrast, chalcopyrite exhibits a strong negative Ir anomaly. On a plot of Os versus Ir (Fig. 6a), pyrrhotite and pentlandite exhibit a positive correlation and fall close to the 1:1 line, indicating that these elements are equally distributed, albeit Os is slightly enriched relative to Ir. Pyrrhotite has the highest concentrations of Os and Ir followed by pentlandite. Chalcopyrite has Os and Ir concentrations close to or below the limit of detection. On a plot of Rh versus Ru (Fig. 6b), pyrrhotite and pentlandite exhibit also a positive correlation and fall close to the 1:1 line, which indicates that these elements are also equally distributed. Pentlandite has the highest concentrations of Ru and Rh. The preference of IPGE and Rh for pyrrhotite and pentlandite is reflecting their compatibility during MSS crystallization. During MSS exsolution it appears that Os and Ir prefer pyrrhotite over pentlandite and Ru and Rh prefer pentlandite over pyrrhotite.

Although Pd is not compatible in MSS and ISS during crystal fractionation of sulfide liquids (Barnes and Lightfoot, 2005 and references therein; Mungall et al., 2005; Brenan, 2008; calculated from Li and Audétat, 2012), its partition coefficient is not 0 and some Pd is present in pentlandite. This has been ascribed to the subsolidus diffusion of Pd from MSS and fractionated liquids into pentlandite (Barnes et al., 2006; Dare et al., 2010). As observed elsewhere (e.g., Medvezky Creek Mine, Noril'sk, Barnes et al., 2006; Merensky Reef, Bushveld Complex, Godel et al., 2007; Platreef, Bushveld Complex, Holwell and McDonald, 2007; J–M Reef, Stillwater Complex, Godel and Barnes, 2008; McCreedy East deposit, Sudbury, Dare et al., 2011; Rosie Nickel Prospect, Yilgarn Craton, Godel et al., 2012; Aguablanca, Piña et al., 2012; Grasvally Norite–Pyroxenite–Anorthosite (GNPA) member, Bushveld Complex, Smith et al., 2014; Jinchuan, Chen et al., 2014), the pentlandite pattern displays a high positive Pd peak (Fig. 4). On plots of Pd versus Rh and Pd versus Ru (Fig. 7a, b), pentlandite exhibits strong correlations, and Pd is enriched by 3 orders of magnitude relative to Rh and Ru. This correlation reflects the diffusion of Pd into pentlandite during its exsolution from MSS. In contrast, pyrrhotite and chalcopyrite do not exhibit any correlation for these elements.

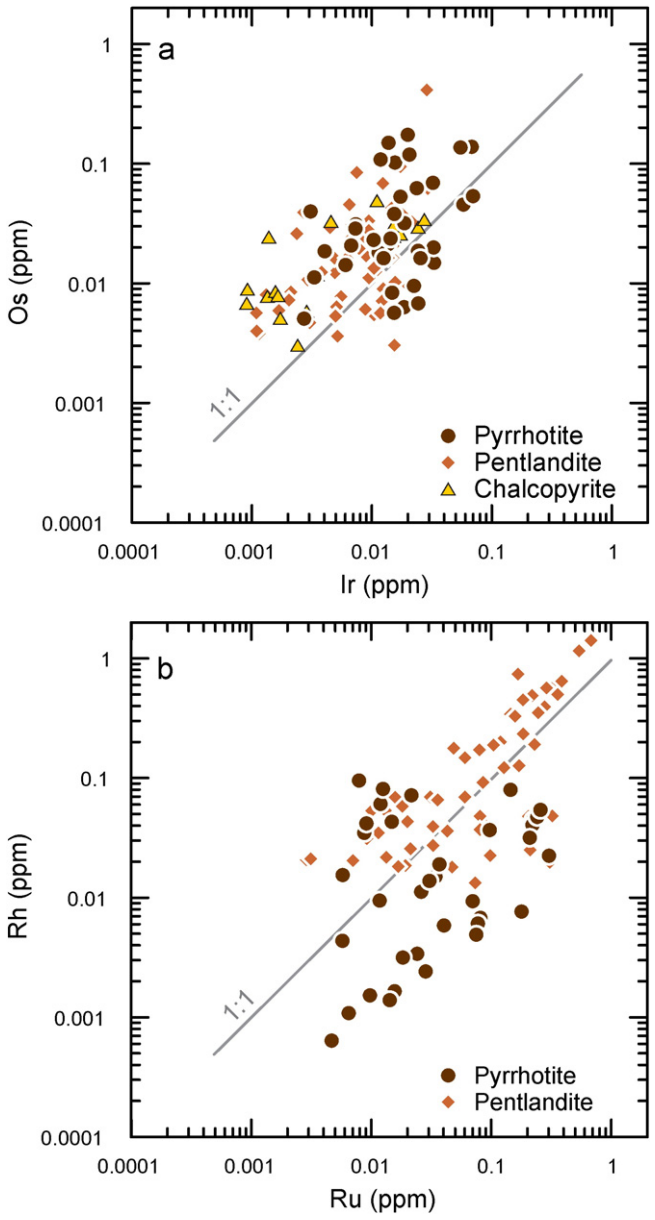

Fig. 6. Binary diagrams: (a) Os versus Ir; and (b) Rh versus Ru. Note the relatively high degree of correlation for sulfides, which follow the 1:1 line on both diagrams. Chalcopyrite analyses are not plotted in panel *b* because of excessive interference between ^{63}Cu and ^{103}Rh.

Unlike Pd, Pt and Au are not commonly found in BMS. They are expected to remain in the late fractionated liquids with the semi-metals (Te, Sb, Bi and As: Barnes and Lightfoot, 2005 and references therein; Mungall et al., 2005; Brenan, 2008; Helmy et al., 2010; calculated from Li and Audétat, 2012; Liu and Brenan, 2015). For all the BMS of the Lac des Iles sulfide-rich pods, Pt and Au are close to or below detection limits and do not correlate with any elements or with each other. This suggests that Pt and Au did not partition into MSS and ISS and should be present in another phase. Given the low Pt and Au concentrations in BMS relative to the whole rock and the presence of Pt-bearing PGM (Duran et al., 2016), we anticipate that Pt and Au are mainly present as distinct discrete minerals such as PGM or electrum. Such phases have also been observed in the disseminated ore (Watkinson and Dunning, 1979; Talkington and Watkinson, 1984; Sutcliffe et al., 1989; Djon and Barnes, 2012).

When MSS crystallizes, Cu, Ag, Cd, and Zn partition into the fractionated liquid because they are not compatible in MSS (e.g., Barnes et al.,

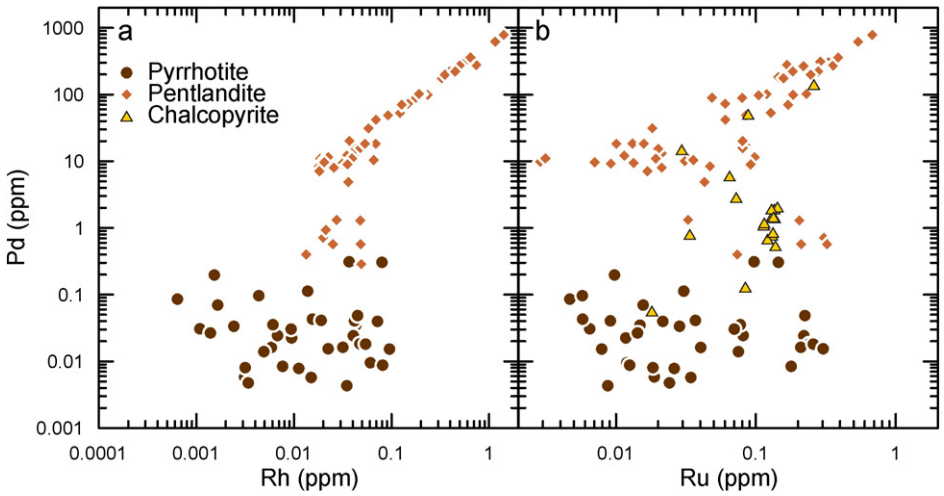

Fig. 7. Binary diagrams: (a) Pd versus Rh; and (b) Pd versus Ru. Note the relatively high degree of correlation for pentlandite on both diagrams. As in panel b of Fig. 6, chalcopyrite analyses are not plotted in panel *a* because of interference between ^{63}Cu and ^{103}Rh.

1997). Upon cooling, these elements partition into ISS, and they are usually found in chalcopyrite (Barnes et al., 2006, 2008). Chalcopyrite exhibits a strong enrichment in Cu and Ag, at around 10,000 times their concentration in the primitive mantle (Lyubetskaya and Korenaga, 2007). In contrast, pyrrhotite and pentlandite exhibit a negative Cu anomaly and have lower Ag values. On plots of Ag versus Cd and Zn (Fig. 8a, b), the BMS do not show a clear correlation, but in general Ag, Cd, and Zn are concentrated in chalcopyrite. Silver concentrations in pentlandite are high (up to 70.3 ppm) and variable, which may be explained by the heterogeneous distribution of Ag.

As in the case of Pt and Au, semi-metals (i.e., Te, Sb, Bi, As) are not compatible in MSS and ISS (Helmy et al., 2010; Liu and Brenan, 2015). The three BMS contain low concentrations of semi-metals and these elements do not correlate with each other or with other elements. Pyrrhotite displays a smoothly increasing pattern from Sn to As (Fig. 4). Pentlandite is characterized by small positive Pb and Bi peaks. The chalcopyrite pattern resembles the pentlandite pattern except for Cd which is highly enriched in chalcopyrite as mentioned previously.

5.2. Fe–Ti oxide compositions

The median composition of each Fe–Ti oxide is presented in Table 2, along with the minimum and maximum values. The full data set is presented in the electronic supplementary material. Typical time–signal diagrams for the Fe–Ti oxides are presented in Fig. 9 and they indicate that the lithophile and chalcophile elements are present in solid solution. In ilmenite, the elements are homogeneously distributed (Fig. 9a, b). Hematite exsolutions in ilmenite (Fig. 2e) are not apparent on the time–signal diagrams owing to their size, which is smaller than the size of the laser beam. In magnetite, most of the elements are homogeneously distributed (Fig. 9c) except for Mg and Al (Fig. 9d), which are preferentially concentrated in spinel lamellae (<50 μm) not visible in thin section.

Magnetite may form in a variety of environments, ranging from high-temperature magmatic to low-temperature hydrothermal environments. As mentioned above, the composition of magnetite depends on the composition of the magmatic liquid (silicate or sulfide) or aqueous fluid from which it crystallizes and the partition coefficient of the elements in magnetite. In addition, its composition depends on the competition between co-crystallizing phases, such as ilmenite and sulfides, for the elements. On this basis, Dare et al. (2014b) developed a multi-element diagram to identify the signatures of magnetite from various environments, with elements plotted from left to right in order of compatibility in magnetite. In the subsequent treatment of

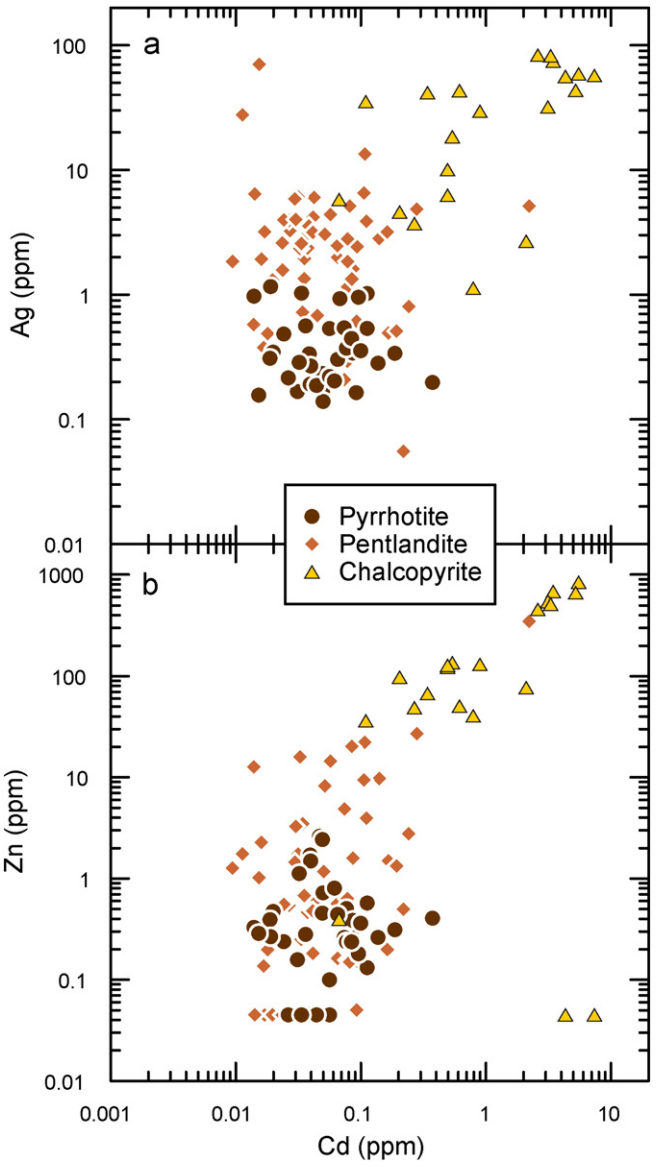

Fig. 8. Binary diagrams: (a) Ag versus Cd; and (b) Zn versus Cd. Note that chalcopyrite is generally enriched in these elements relative to pyrrhotite and pentlandite.

Table 2
Compositions of Fe–Ti oxides from Lac des Iles sulfide-rich pods as determined by LA–ICP-MS analysis.

Element		Isotope	Magnetite			Ilmenite		
			n = 55			n = 25		
			Median	Min	Max	Median	Min	Max
Mg	(ppm)	^{25}Mg	182	46.3	2930	284	68.2	1731
Al	(ppm)	^{27}Al	1196	518	6768	101	18.6	1046
Si	(ppm)	^{29}Si	1094	≤648	8856	1957	766	4505
Ca	(ppm)	^{44}Ca	18.0	≤12.3	744	125	15.9	2130
Sc	(ppm)	^{45}Sc	1.18	0.403	3.67	288	44.7	332
Ti	(ppm)	^{47}Ti	506	96.4	3305	273,921	230,140	294,189
V	(ppm)	51V	5200	27.8	21,800	2467	566.1	6238
Cr	(ppm)	^{52}Cr	596	5.04	13,530	298	4.51	1852
Mn	(ppm)	^{55}Mn	2583	222	2987	8189	5177	17,043
Co	(ppm)	^{59}Co	22.3	7.34	166	11.0	1.22	182
Ni	(ppm)	^{60}Ni	596	237	1145	41.0	11.7	1322
Cu	(ppm)	^{63}Cu	1.10	0.083	1901	2.66	1.68	1689
Zn	(ppm)	^{66}Zn	28.9	9.28	1305	37.2	19.0	169
Ga	(ppm)	^{71}Ga	48.9	18.2	125	0.825	0.454	3.79
Ge	(ppm)	^{74}Ge	0.799	0.443	1.29	≤0.125	≤0.125	0.445
Y	(ppm)	^{89}Y	≤0.013	≤0.013	0.288	0.221	0.068	1.36
Zr	(ppm)	^{90}Zr	0.028	≤0.015	0.375	6.57	0.610	176
Nb	(ppm)	^{93}Nb	≤0.018	≤0.018	1.41	29.2	9.93	125
Mo	(ppm)	^{95}Mo	≤0.143	≤0.143	0.471	0.899	0.318	2.12
Sn	(ppm)	^{118}Sn	0.454	0.080	11.6	1.71	0.211	32.56
Hf	(ppm)	^{178}Hf	≤0.015	≤0.015	0.028	0.562	0.041	6.28
Ta	(ppm)	^{181}Ta	≤0.006	≤0.006	0.174	1.56	0.185	8.06
W	(ppm)	^{182}W	≤0.015	≤0.015	1.07	2.39	0.180	25.7
Pb	(ppm)	^{208}Pb	0.116	0.020	5.76	0.192	≤0.011	0.913

n = number of analysis; min = minimum value; max = maximum value.

the data we present the elements in increasing order of compatibility in magnetite (Fig. 10).

Considering the multi-element patterns from incompatible to compatible elements in magnetite, we note an increasing slope for both oxides (Fig. 10). Typically, magmatic magnetite is relatively depleted in the least compatible elements, such as Si and Ca, which are present when magnetite forms from hydrothermal fluids (Dare et al., 2014b; Nadoll et al., 2014). In magnetite from the Lac des Iles sulfide-rich pods, the Si and Ca concentrations are close to or below the detection limit. Similarly, Si concentrations in ilmenite are close to the detection

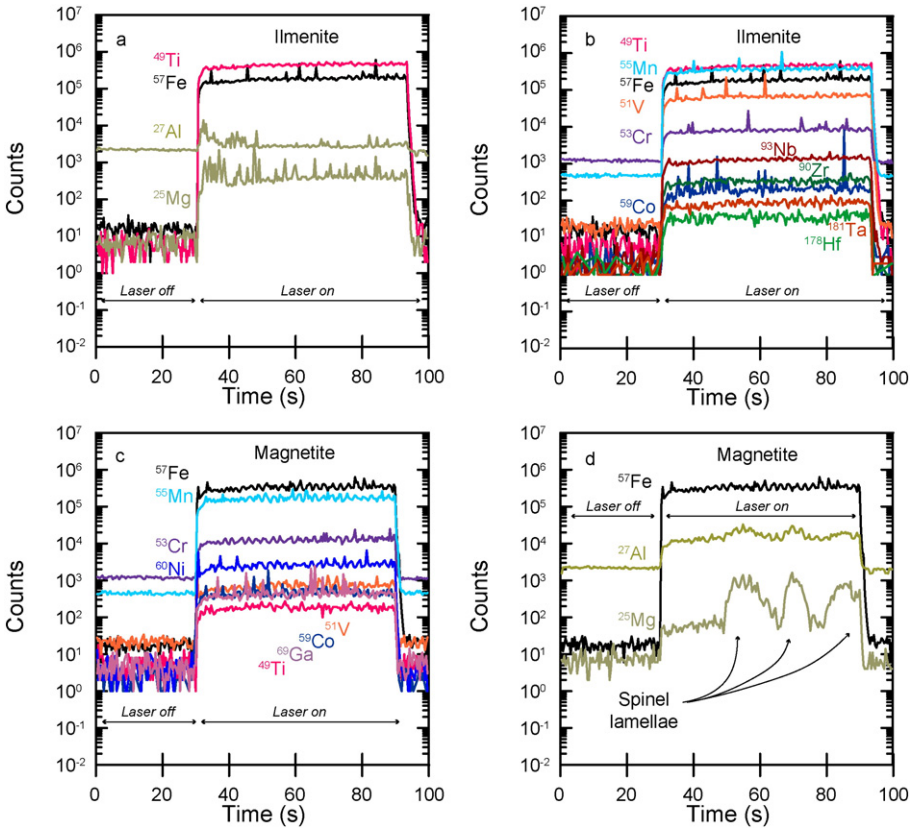

Fig. 9. Examples of time–signal diagrams for Fe–Ti oxides: (a–b) ilmenite; (c–d) magnetite. Note that spinel lamellae are present in some magnetites.

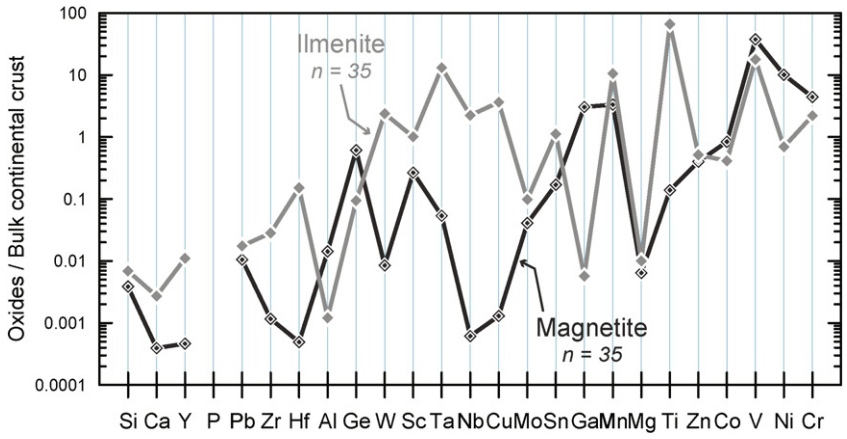

Fig. 10. Bulk continental crust normalized multi-element diagram of magnetite and ilmenite from Lac des Iles sulfide-rich pods. The normalization values are from Rudnick and Gao (2003).

limit, but Ca concentrations are in the range of 15.9 to 2130 ppm with most values <1000 ppm. Both observations suggest that the magnetite and ilmenite associated with Lac des Iles sulfide-rich pods did not form from an aqueous fluid.

In contrast, magmatic magnetite is relatively enriched in Al, Mn, high field strength elements (HFSE; Zr, Hf, Ta, and Nb), Sc, W, and Ti (Dare et al., 2014b). These elements are considered relatively immobile in aqueous fluids and are depleted in hydrothermal magnetite (Nadoll et al., 2014). In magnetite from the Lac des Iles sulfide-rich pods, the Al and Mn concentrations are quite high, in the range of 222 to 6768 ppm, but the concentrations of Ti are low, <1 wt.%. The concentrations of HFSE, Sc, and W are also low (<1 ppm). The low Ti, HFSE, Sc, and W values are especially apparent on the magnetite multi-element pattern (Fig. 10), which shows Hf, W, and Nb negative anomalies. These low values contradict the interpretation, based on Si, Ca, Al, and Mn, that the magnetite is igneous. This contradiction may be resolved by considering the presence of ilmenite. In the Sept.-Iles layered intrusion and in the Lac Saint-Jean anorthosite it has been demonstrated that, during co-crystallization of both Fe–Ti oxides, ilmenite preferentially includes HFSE, Sc, and W, whereas magnetite preferentially accommodates Al, Ga, Mg, Ni, and Cr (Méric, 2011; Néron, 2012). The Fe–Ti oxides from the Lac des Iles sulfide-rich pods exhibit a similar behavior, with magnetite being depleted in HFSE, Sc, and W whereas ilmenite exhibits an enrichment in these elements (Fig. 10).

Magmatic magnetite may also be fairly enriched in some chalcophile elements, such as Pb, Cu, Mo, Sn, Zn, and Co (Dare et al., 2012, 2014b). However, just as co-crystallization of ilmenite impoverishes magnetite in Ti, HFSE, Sc, and W, sulfide segregation prior to crystallization of oxides affects the chalcophile element composition of the oxides. The concentrations of Pb, Cu, Mo, Sn, Zn, and Co are relatively low in both magnetite and ilmenite (Fig. 10). Cobalt and Zn are the only elements for which the concentrations may exceed hundreds of ppm. The other elements have concentrations of <33 ppm. The low overall abundance of these chalcophile elements in oxides may reflect their partitioning into sulfides in preference to oxides. However, Sn concentrations in sulfides are not much higher than in oxides. This has also been noticed at Sudbury (Dare et al., 2012) and suggests that Sn partitions similarly into both sulfides and oxides.

Vanadium, Ni, and Cr are usually the most enriched elements in magmatic magnetite whereas they are depleted in hydrothermal magnetite (Dare et al., 2014b; Nadoll et al., 2014). In magnetite from the Lac des Iles sulfide-rich pods, the Cr and V concentrations are extremely variable ranging from 5.04 ppm to 2.18 wt.%. Nickel concentrations are less variable, ranging from 237 to 1145 ppm for magnetite and 11.7 to 1322 ppm for ilmenite. On the multi-element diagram of magnetite, the median values of V, Ni, and Cr are greater than 10 times the value of the bulk continental crust, which indicates strong enrichment of these elements (Fig. 10). The ilmenite pattern for V, Ni, and Cr is similarly shaped but lower, which indicates the partitioning of these elements between magnetite and ilmenite. On a plot of Cr versus V (Fig. 11), a correlation between these elements for both magnetite and ilmenite can be observed. This trend has been observed at other localities (e.g., Sudbury, Voisey's Bay, and Noril'sk) and has been interpreted to result from sulfide liquid fractionation (Dare et al., 2012; Boutroy et al., 2014). Vanadium and Cr are compatible elements in magnetite and do not partition into sulfides. Therefore, the minor amounts of these elements that are present in sulfide liquids are concentrated in magnetite that crystallizes early, thus depleting the fractionated liquids. Consequently, late-crystallizing magnetite is impoverished in these elements relative to early-crystallizing magnetite. In contrast, Ni is slightly incompatible in MSS at high temperature (Li et al., 1996; Mungall et al., 2005), and some Ni partitions into early-crystallizing magnetite (Dare et al., 2012). Upon cooling, Ni becomes incompatible in the fractionated liquid (Li et al., 1996; Mungall et al., 2005), such that some Ni partitions into late-crystallizing magnetite (Dare et al., 2012). Thus, the Ni concentration remains fairly constant in sulfide liquids during crystal fractionation. The variable Cr and V concentrations and the constant Ni concentration suggest to us that Fe–Ti oxide compositions changed with the crystal fractionation of sulfide liquids.

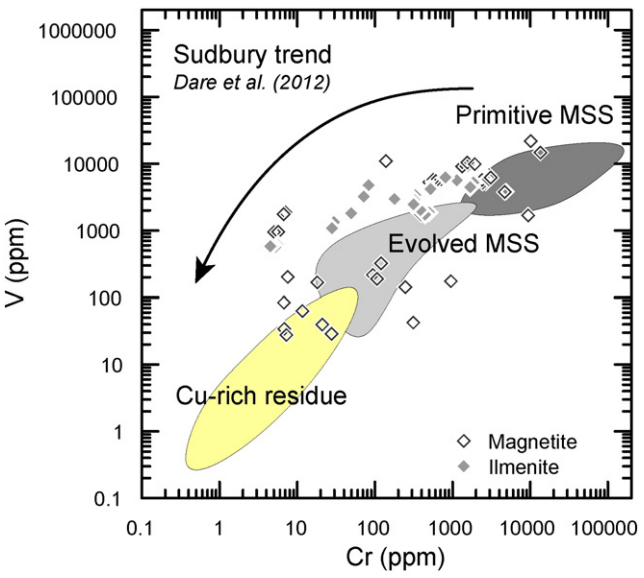

Fig. 11. Binary diagram of V versus Cr. Note that the data set follows the trend of sulfide fractionation defined by Dare et al. (2012).

Magnetites with low concentrations of V and Cr could be interpreted as having a hydrothermal signature rather than being the product of crystallization from evolved sulfide liquids. The plot of Ni + Cr versus Si + Mg developed by Dupuis and Beaudoin (2011) may be used to discriminate magnetites from magmatic Ni–Cu–PGE deposits and hydrothermal deposits (Dare et al., 2012; Boutroy et al., 2014). This plot shows that, although magnetites within Lac des Iles sulfide-rich pods show variable degrees of fractionation and depletion in some compatible elements, most of them do not plot outside of the field of Ni–Cu–PGE deposits, thus confirming the magmatic origin of the magnetite (Fig. 12).

5.3. Degree of fractionation of the parental magma

In mafic–ultramafic igneous systems, the PGE and chalcophile elements are commonly assumed to be scavenged from silicate magmas by sulfide liquids, which are formed when the silicate magma reaches sulfur saturation (e.g., Naldrett, 2004). The amount of PGE and chalcophile elements collected by sulfide liquids are controlled by two parameters: (1) the concentrations of the PGE and chalcophile elements in the silicate magma; and (2) the silicate to sulfide ratio (i.e., R-factor: Campbell and Naldrett, 1979).

The amount of PGE and chalcophile elements that are available at the time of sulfide segregation are directly related to the degree of fractionation of the magma (Barnes et al., 1985). Sulfides derived from magmas with similar degrees of fractionation should have similar patterns on primitive mantle normalized metal diagrams. However, sulfides derived from similar magmas but with different R-factors will not have the same composition, especially for PGE. Barnes and Lightfoot (2005) demonstrated that massive sulfides at many localities have lower PGE concentrations than disseminated sulfides, possibly because of a lower R-factor. This difference arises because PGE have the highest partition coefficients for sulfides. Nonetheless, because they have similar partition coefficients (Barnes and Lightfoot, 2005 and references therein; Mungall et al., 2005; Brenan, 2008; calculated from Li and Audétat, 2012) the degree of fractionation of all the PGE will be similar regardless of the R-factor. For example, when comparing the pyrrhotite and pentlandite from the Lac des Iles sulfide-rich pods with the pyrrhotite and pentlandite from the Lac des Iles disseminated mineralization (Djon and Barnes, 2012), similar patterns are found (Fig. 13). However, the minerals from the disseminated mineralization are slightly richer in all the elements than the minerals from the sulfide-rich pods. This difference could be the result of a higher R-factor for the disseminated mineralization as proposed by Duran et al. (2016), and demonstrates that sulfides from sulfide-rich pods and those from disseminated sulfides are derived from a similar parental magma.

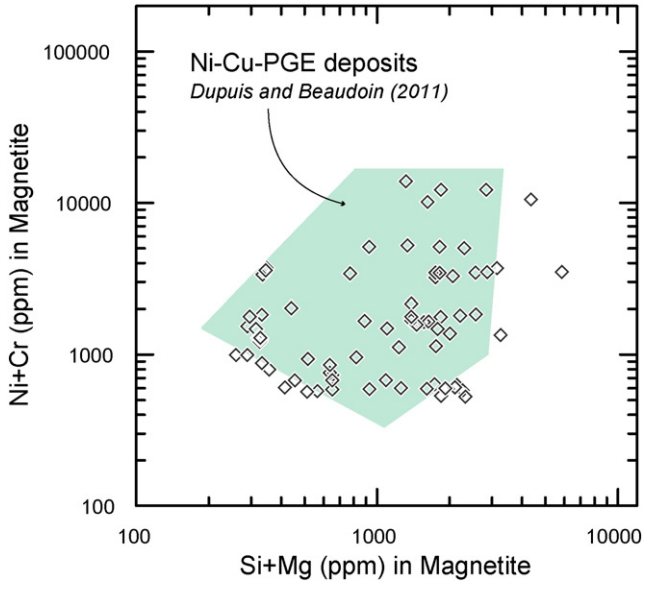

Fig. 12. Binary diagram of Ni + Cr versus Si + Mg in magnetite. Note that the data set plots within the field of Ni–Cu–PGE deposits defined by Dupuis and Beaudoin (2011).

According to Barnes and Gomwe (2010) the parental magmas of the Lac des Iles deposits were andesites (i.e., evolved magmas) emplaced into a convergent plate margin setting (Brügmann et al., 1997). To test this hypothesis, we plotted the pyrrhotite and pentlandite trace element composition from Lac des Iles in comparison with those emplaced in stable cratons or rifted intraplate margins and derived from more primitive magmas, and those emplaced in convergent setting and/or derived from more evolved magmas.

The trace element signatures of pyrrhotite and pentlandite from the Lac des Iles sulfide-rich pods appear to be different from those of Ni–Cu–PGE deposits emplaced in stable cratons or rifted intraplate areas and derived from primitive magmas. For instance, the pyrrhotites and pentlandites from layered intrusions such as the Bushveld Complex, the Stillwater Complex and the Great Dyke (Godel et al., 2007; Holwell and McDonald, 2007; Barnes et al., 2008; Godel and Barnes, 2008; Smith et al., 2014), from komatiites such as the Rosie Nickel Prospect (Godel et al., 2012), from ultramafic intrusions such as Jinchuan (Chen et al., 2014) and from flood basalts such as Noril'sk (Barnes et al., 2006) are much richer in most of the elements, particularly in the IPGE, relative to the pyrrhotite and pentlandite from Lac des Iles (Fig. 14a-d). Furthermore, the pentlandite from Lac des Iles has a higher Pd/Ir value, which supports the idea that the MSS formed from a fractionated magma because fractionated magmas have high Pd/Ir values, whereas primitive ones do not (Barnes et al., 1985). These observations suggest that the trace element signature of the sulfides may be influenced by the degree of fractionation of the magma from which they formed.

The trace element signatures of pyrrhotite and pentlandite from Lac des Iles appear to be similar to those of Ni–Cu–PGE deposits emplaced in convergent settings and/or derived from evolved magmas. For instance, Aguablanca magmas formed in an arc setting, which might be similar to the setting of Lac des Iles (Brügmann et al., 1997), and Sudbury magmas have an average andesitic composition (Rudnick and Gao, 2003) as a meteorite impact flash-melted the bulk continental crust (Golightly, 1994). Both of these deposits originated from evolved magmas, and the concentrations of PGE and chalcophile elements in pyrrhotite and pentlandite from Lac des Iles are close to those of pyrrhotite and pentlandite from Aguablanca (Piña et al., 2012; Fig. 14e-f) and Sudbury (Dare et al., 2011; Fig. 14e-f). These observations are consistent with the parental magmas of Lac des Iles having been of andesitic affinity. This approach could then be applied to less well understood examples to infer the degree of fractionation of the magmas from which sulfides formed (and thus infer the tectonic environment in which the magmas were likely emplaced).

Magnetite and ilmenite from the Lac des Iles sulfide-rich pods also show similar patterns to magnetite and ilmenite from Sudbury on a bulk continental crust normalized multi-element diagram (Fig. 15). The magnetite from the Lac des Iles sulfide-rich pods is particularly similar to magnetite derived from the more evolved part of Sudbury (i.e., McCreedy East) except in terms of HFSE because the magnetite from McCreedy East did not co-crystallize with ilmenite. This similarity may suggest a similar origin for both oxides from Lac des Iles sulfide-rich pods and McCreedy East (i.e., derived from evolved magmas).

5.4. Timing of crystallization of Fe–Ti oxides

The recording of crystal fractionation in the composition of magnetite (Cr and V variations, Fig. 11) suggests that magnetite crystallized after the sulfide liquids formed. This interpretation is supported by normalizing the composition of magnetite from the Lac des Iles sulfide-rich pods to the composition of magnetite crystallized from andesitic magmas that did not reach S saturation (Dare et al., 2014b). The

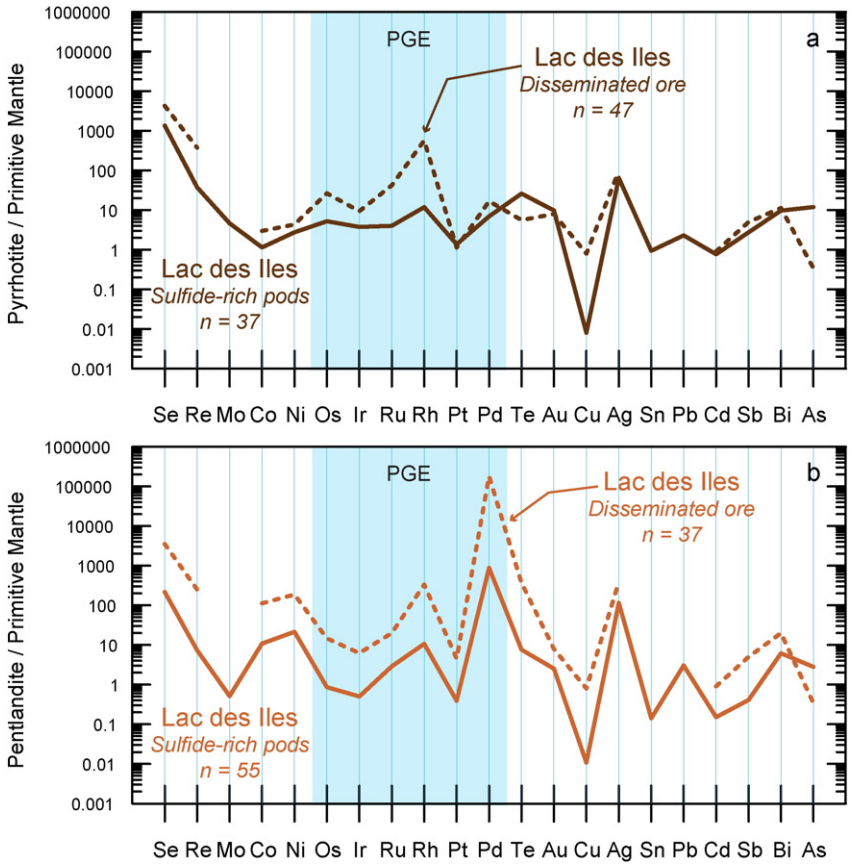

Fig. 13. Primitive mantle normalized multi-element diagrams of (a) pyrrhotite and (b) pentlandite from Lac des Iles sulfide-rich pods compared with Lac des Iles disseminated sulfides (dashed lines). The data for disseminated sulfides are from Djon and Barnes (2012). The normalization values are from Lyubetskaya and Korenaga (2007).

magnetite associated with Lac des Iles sulfide-rich pods is depleted in all of the chalcophile elements relative to the magnetite from andesites that contain no sulfides (Fig. 16), thereby suggesting that magnetite associated with sulfide-rich pods crystallized after the magmas reached S saturation.

In contrast to magnetite associated with Lac des Iles sulfide-rich pods, magnetite from andesites analyzed by Dare et al. (2014b) did not co-crystallize with ilmenite. Our results demonstrate that magnetite from the Lac des Iles sulfide-rich pods is depleted in Ti and HFSE relative to magnetite from andesites owing to the co-crystallization of ilmenite (Fig. 16).

Experimental studies (Naldrett, 1969; Kress et al., 2008) indicate that up to 15% magnetite can crystallize from sulfide liquids and magnetite and ilmenite are often present in minor amounts in magmatic sulfides (e.g., Lesher and Keays, 2002; Tomkins et al., 2012; Dare et al., 2012). However, direct crystallization of ilmenite from sulfide liquids is difficult to address given the paucity of experimental data on the partitioning of Ti into sulfide liquids. Alternatively, magnetite and ilmenite could have formed as O diffused out of sulfide liquids and reacted with surrounding silicate liquids (Fonseca et al., 2008). In both cases, Fe–Ti-oxides formed from sulfide liquids while sulfide minerals were crystallizing.

5.5. Exsolution of MSS

In magmatic Ni–Cu–PGE deposits pyrrhotite and pentlandite represent exsolution products of MSS that form during cooling (Naldrett, 1969; Craig, 1973). Numerous studies have demonstrated that pyrrhotite and pentlandite usually accommodate significant amounts of the whole-rock IPGE composition (i.e., Aguablanca, Piña et al., 2012; McCreedy East deposit, Sudbury, Dare et al., 2011; Main Sulfide Zone, Great Dyke, Barnes et al., 2008; J–M Reef, Stillwater Complex, Godel and Barnes, 2008; Merensky Reef, Platreef, and GNPA member, all of which are part of the Bushveld Complex, Godel et al., 2007; Holwell and McDonald, 2007; Smith et al., 2014, respectively; Rosie Nickel Prospect, Yilgarn Craton, Godel et al., 2012; Medvezky Creek Mine, Noril'sk, Barnes et al., 2006; Jinchuan, Chen et al., 2014). The distributions of IPGE between pyrrhotite and pentlandite from the Lac des Iles sulfide-rich pods are similar, which supports the hypothesis that pyrrhotite and pentlandite were exsolved from MSS.

To test whether exsolution of pyrrhotite and pentlandite from MSS would redistribute the IPGE in the same manner in various environments, we have plotted the composition of each IPGE in pyrrhotite versus the composition in pentlandite for different Ni–Cu–PGE deposits (Fig. 17). On a plot of Ir in pyrrhotite versus Ir in pentlandite we notice that Lac des Iles sulfide-rich pods lie close to the 1:1 line, as do most of the other Ni–Cu–PGE deposits. Osmium and Ru exhibit trends that are similar to that of Ir (Fig. 17a-c). This result indicates that, during the development of pyrrhotite and pentlandite, the IPGE are equally distributed between pyrrhotite and pentlandite. However, the J–M Reef of the Stillwater Complex does not follow this trend, instead pentlandite is enriched in IPGE relative to pyrrhotite by a factor of 10. In contrast with IPGE, Rh shows variable distributions between pyrrhotite and pentlandite, depending on the deposits (Fig. 17d). Most deposits plot close to the 1:1 line, but the Platreef and Merensky Reef of the Bushveld Complex show a 30:1 enrichment of Rh in pentlandite and the J–M Reef of the Stillwater Complex shows a 250:1 enrichment.

Although Ag is incompatible in MSS, we also note that in the pentlandite from Lac des Iles and in those from other deposits (i.e., Aguablanca, Piña et al., 2012; McCreedy East deposit, Sudbury, Dare et al., 2011; Main Sulfide Zone, Great Dyke, Barnes et al., 2008; J–M Reef, Stillwater Complex, Godel and Barnes, 2008; Merensky Reef, Bushveld Complex,

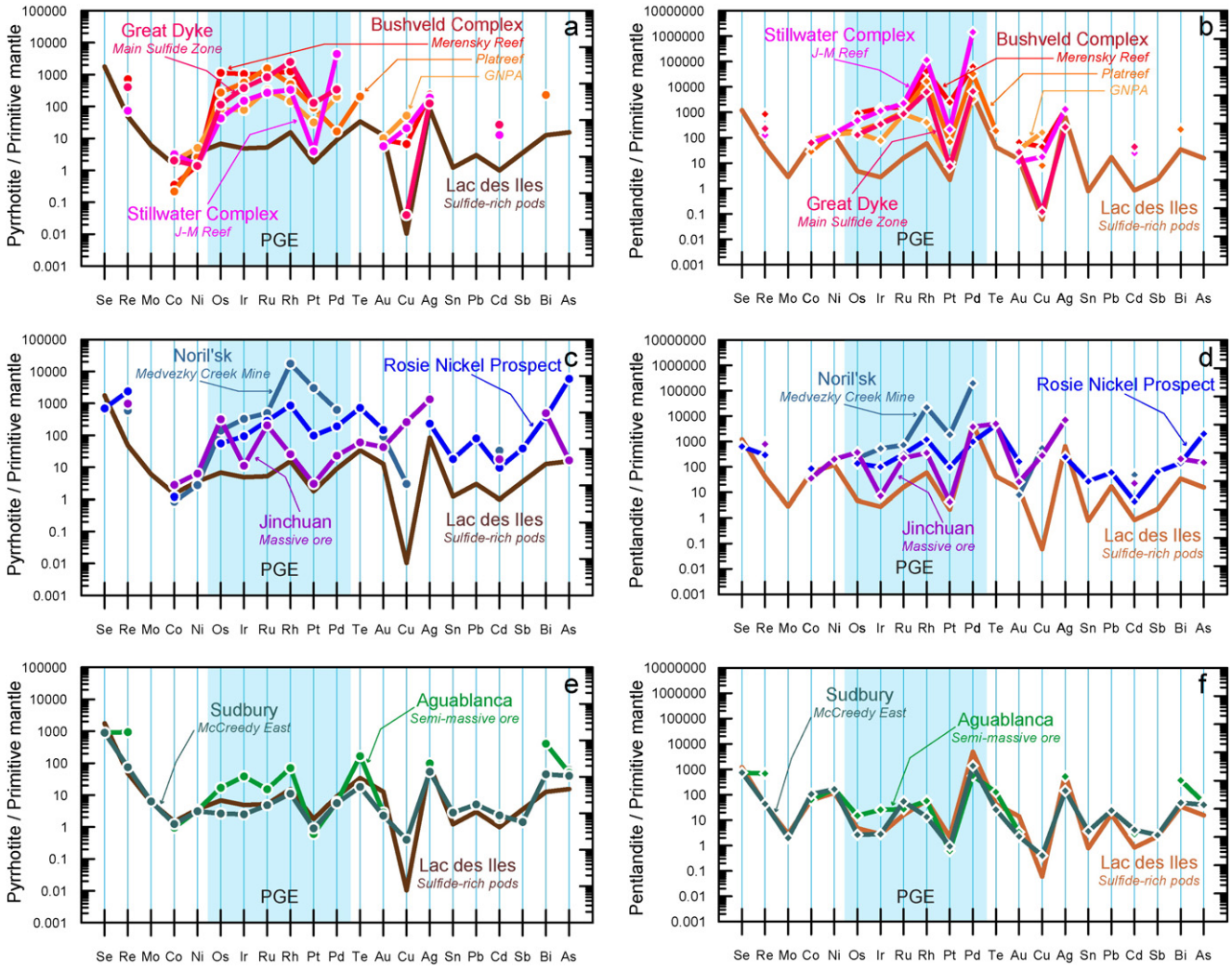

Fig. 14. Primitive mantle normalized multi-element diagrams of pyrrhotite and pentlandite from Lac des Iles sulfide-rich pods compared with pyrrhotite and pentlandite from (a–b) Great Dyke, Main Sulfide Zone, (Barnes et al., 2008); Stillwater Complex, J–M Reef (Godel and Barnes, 2008); Merensky Reef (Godel et al., 2007), Platreef (Holwell and McDonald, 2007) and GNPA member (Smith et al., 2014) from the Bushveld Complex, (c–d) Rosie Nickel Prospect (Godel et al., 2012); Noril'sk, Medvezky Creek Mine (Barnes et al., 2008); Jinchuan, massive ore (Chen et al., 2014), (e–f) Aguablanca, semi-massive ore (Piña et al., 2012); Sudbury, McCreedy East (Dare et al., 2011). The normalization values are from Lyubetskaya and Korenaga (2007).

Godel et al., 2007; Rosie Nickel Prospect, Yilgarn Craton, Godel et al., 2012; Jinchuan, Chen et al., 2014), Ag is present in significant concentrations. Furthermore, in most deposits Ag is enriched in pentlandite relative to pyrrhotite by factors of 5 to 10 (Fig. 18). This could be a consequence of Ag diffusion during exsolution of pentlandite from MSS in the same manner as Ni, Co, and Pd.

5.6. Deformation

Only a few studies have paid attention to the role of deformation in redistributing certain elements at the grain scale. These include studies of metamorphosed sulfides from Penikat in Finland (Barnes et al., 2008), Raglan in Canada (Misson et al., 2013), some komatiites from the Yilgarn Craton in Australia (Vukmanovic et al., 2014), and the Limoeiro magma conduit in Brazil (Mota-e-Silva et al., 2015).

Metamorphism is believed to promote diffusion of some elements when the sulfides recrystallize. Whereas IPGE are homogeneously distributed within pyrrhotite and pentlandite from unmetamorphosed Ni–Cu–PGE deposits, Barnes et al. (2008) noticed that the IPGE distribution within pyrrhotite and pentlandite from the PV Reef of the Penikat Intrusion, which has undergone greenschist facies metamorphism, was not homogeneous. Moreover, they observed that inclusions of PGM composed of IPGE were more abundant than in unmetamorphosed deposits. We did not observe such PGM in the BMS from the Lac des Iles sulfide-rich pods. Instead, the IPGE are homogeneously distributed within the pyrrhotite and pentlandite. Therefore, metamorphism is unlikely to have affected the IPGE distribution in the sulfide-rich pods.

Similarly, Pd and Rh are systematically homogeneously distributed in pentlandite, as indicated by the time–signal diagrams in Fig. 3. Given this consideration, we may argue that deformation did not contribute to redistributing the Pd and Rh at Lac des Iles.

However, Vukmanovic et al. (2014) demonstrated that the concentrations of some elements such as Ag, Bi, and Pb, increase along certain grain boundaries, low-angle boundaries, and twin boundaries within pyrrhotite grains. This observation was limited to the elements with large ionic radii, which might have been redistributed more easily. Vukmanovic et al. (2014) suggested that deformation-controlled diffusion could occur at temperatures as low as 350 °C, which is consistent with greenschist facies conditions. Similarly, we observed heterogeneous distribution of these elements within some pyrrhotite and in most pentlandite (Fig. 3). This is especially apparent on the chemical maps (Fig. 19), where Ag and Pb are more concentrated along cracks and grain boundaries. Furthermore, a heterogeneous distribution of these elements is observed within coarse pentlandite, which is likely

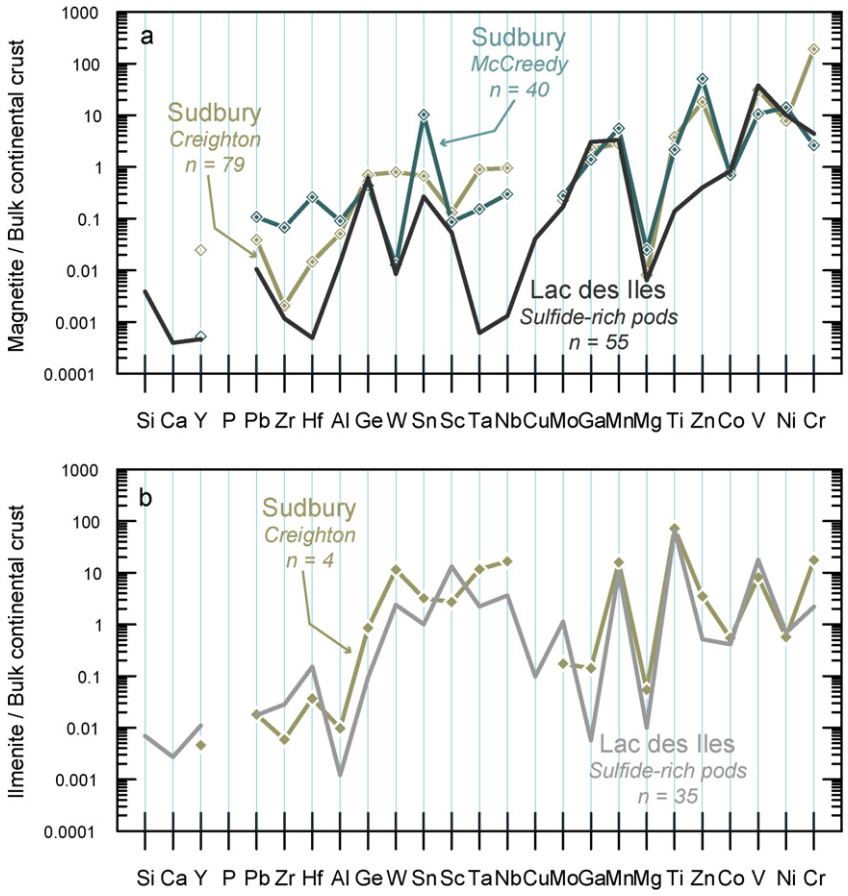

Fig. 15. Bulk continental crust normalized multi-element diagrams of (a) magnetite and (b) ilmenite from Lac des Iles sulfide-rich pods and Sudbury. The data from Sudbury are from Dare et al. (2012). The normalization values are from Rudnick and Gao (2003).

to have formed at approximately 600 °C (Naldrett, 1969). Given these considerations, the initial distribution of Ag, Bi, and Pb in pentlandite may have been modified during deformation under greenschist conditions.

Alternatively, these metals could have been introduced by fluids as Ag and Pb can form stable complexes with HS^- and Cl^- in magmatic-hydrothermal systems (e.g., Pokrovski et al., 2013). Circulation of fluids along the deformation planes in the sulfides could have allowed incorporation of these metals along cracks and grain boundaries.

5.7. Application to exploration and future directions

We suggest that the composition of pentlandite from PGE-dominated deposits (Bushveld Complex: Holwell and McDonald (2007), Godel et al. (2007), and Smith et al. (2014); Stillwater Complex: Godel and Barnes (2008); Great Dyke: Barnes et al. (2008) and Oberthür et al. (1997); Noril'sk: Barnes et al. (2006); and Lac des Iles: Djon and Barnes (2012) and this study) can be distinguished from pentlandite from Ni–Cu sulfide deposits (Sudbury: Dare et al. (2011); Aguablanca: Piña et al. (2012);

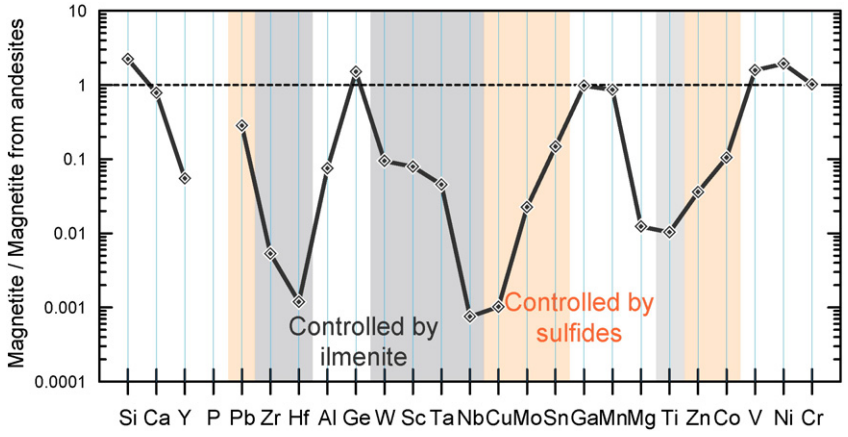

Fig. 16. Multi-element diagram of magnetite from Lac des Iles sulfide-rich pods normalized to magnetite from andesites (values from Dare et al., 2014b). Note that magnetite from Lac des Iles sulfide-rich pods is depleted in chalcophile elements (light-red field) and HFSE (gray field) relative to magnetite from andesites.

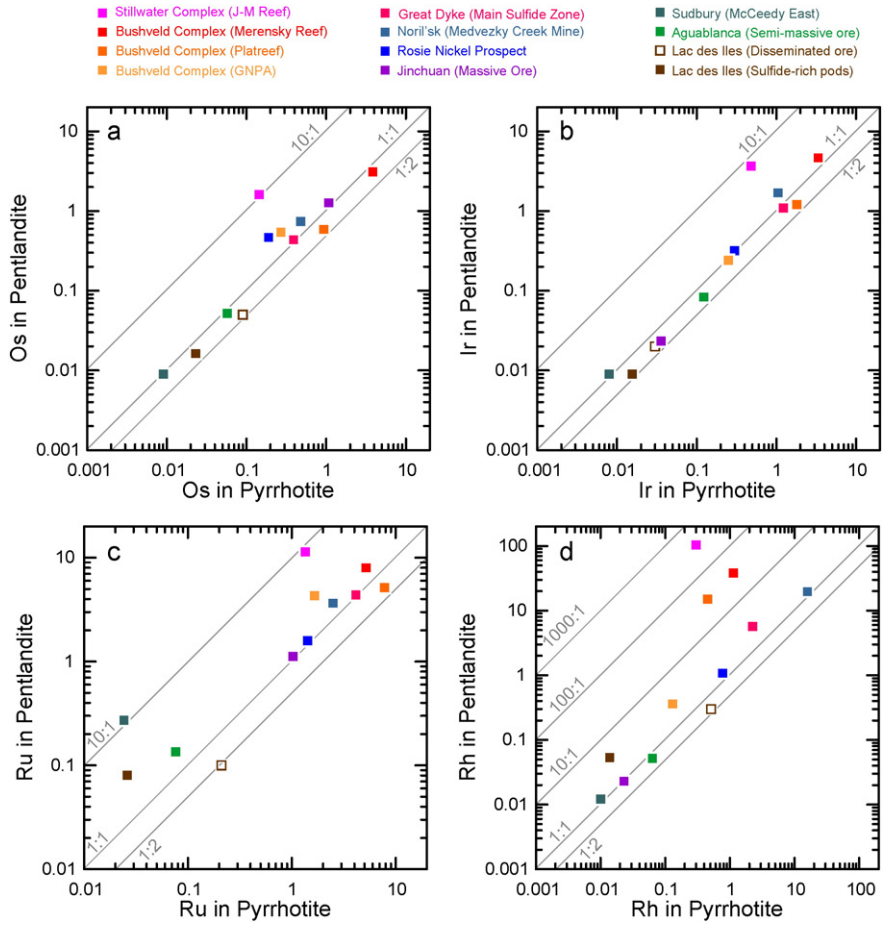

Fig. 17. Binary diagrams of PGE in pentlandite versus PGE in pyrrhotite. (a) Os in pentlandite versus Os in pyrrhotite; (b) Ir in pentlandite versus Ir in pyrrhotite; (c) Ru in pentlandite versus Ru in pyrrhotite; (d) Rh in pentlandite versus Rh in pyrrhotite. The data sources for other Ni–Cu–PGE deposits are: Holwell and McDonald (2007), Godel and Barnes (2008), Barnes et al. (2008), Dare et al. (2010), Djon and Barnes (2012), Piña et al. (2012), Godel et al. (2012), Smith et al. (2014), and Chen et al. (2014).

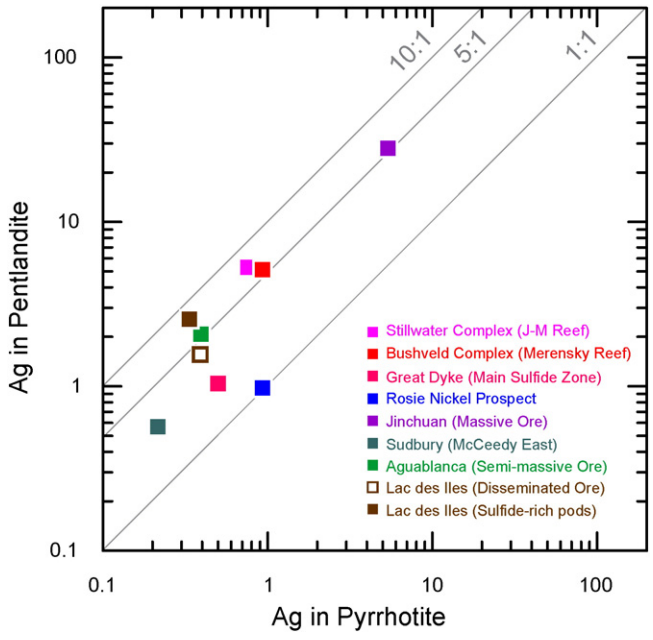

Fig. 18. Binary diagram of Ag in pentlandite versus Ag in pyrrhotite. The data sources for other Ni–Cu–PGE deposits are: Godel and Barnes (2008), Barnes et al. (2008), Dare et al. (2010), Djon and Barnes (2012), Piña et al. (2012), Godel et al. (2012), Chen et al. (2014).

Jinchuan: Chen et al. (2014); and Rosie Nickel Prospect: Godel et al. (2012)). Most pentlandite from PGE-dominated deposits has Pd concentrations of >10 ppm (up to 20,000 ppm for the JM Reef of the Stilwater Complex) whereas pentlandite from Ni–Cu sulfide deposits has Pd concentrations of <10 ppm. Moreover, pentlandite from PGE-dominated deposits has Rh concentrations of >1 ppm, whereas pentlandite from Ni–Cu sulfide deposits has Rh concentrations of <1 ppm. An exception to this is the pentlandite from Lac des Iles that has Rh concentrations comprised between 0.01 and 1 ppm. However, pentlandite from Lac des Iles is still distinguishable from pentlandite of Ni–Cu sulfide deposits based on its higher Pd concentrations. A plot of Pd in pentlandite versus Rh in pentlandite (Fig. 20) may be used to discriminate between PGE-dominated and Ni–Cu sulfide deposits.

As the discovery of near-surface ore deposits is decreasing, targeting deeply buried ore deposits has become critical in modern mineral exploration. Thus, there is a significant need to develop methods that could be added to the exploration geologist toolbox. For example, indicator minerals from glaciated terrains can be used as pathfinders for underlying mineral deposits (McClenaghan, 2005; McClenaghan et al., 2014), and this method has proven very effective in exploration for a wide range of mineral deposits (Averill, 2001), including Ni–Cu–PGE deposits. The presence of olivine, pyroxene, oxide, sulfide, and PGM in tills has been regarded as an indicator for mafic–ultramafic systems and potential Ni–Cu–PGE mineralization (Averill, 2001, 2011; McClenaghan and Cabri, 2011; McClenaghan et al., 2011). Because magnetite is the most widespread and resistive of these indicator minerals, it has been the most closely investigated so far, and the trace element composition of magnetite has been used to established

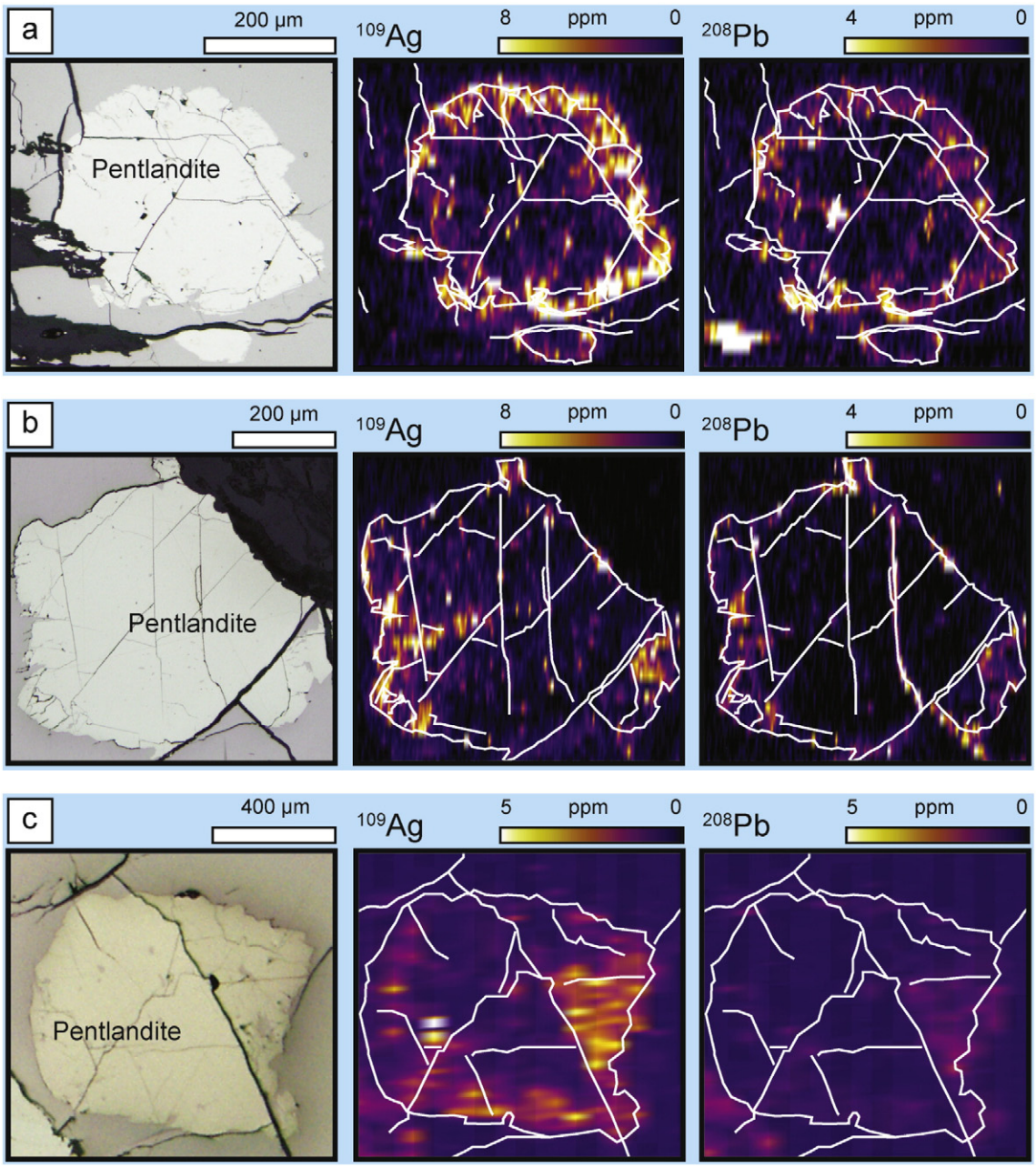

Fig. 19. LA–ICP-MS elemental maps showing the distribution of Ag and Pb in coarse grained pentlandite. (a) Ag and Pb are concentrated along the grain boundaries; (b–c) Ag and Pb are concentrated along cracks and grain boundaries. Note that grain boundaries and cracks are outlined in white.

discriminants as guides for Ni–Cu–PGE exploration (Dupuis and Beaudoin, 2011; Dare et al., 2012, 2014b; Boutroy et al., 2014). Although sulfide minerals are less resistive to mechanical abrasion and chemical weathering than oxide minerals, they can survive in glaciated terrains where chemical weathering is limited and burial is fast due to effective erosion by ice sheets. For instance, McClenaghan et al. (2011) recovered up to 50,000 pentlandite grains from 10 kg of till samples from the Thompson Nickel Belt in central Canada. This approach has a strong potential for exploration across Canada, Greenland, Scandinavia, and Siberia where glaciated terrains represent large areas.

In the last decade, advances in LA–ICP-MS have made such sophisticated tool more readily available. Although LA–ICP-MS is not yet designed for routine exploration, selected samples could be analyzed with a specific purpose. For instance, if pentlandite grains could be recovered from the heavy mineral fraction of till samples, they could be mounted in epoxy, which would allow fast analysis of a large number of grains at relatively low cost. The discrimination diagram that we have developed based on the Pd and Rh compositions of pentlandite found in PGE-dominated and Ni–Cu sulfide deposits need to be tested on pentlandite grains from till surrounding the deposits. Ultimately, this approach could be used in Greenfield programs to provide further insights and identify targets. This is important in the selection of appropriate exploration technics because Ni–Cu sulfide deposits may be detected by geophysical methods whereas PGE-dominated deposits may not be.

6. Concluding remarks

We used LA–ICP-MS to highlight the distribution of trace elements among primary BMS and the associated Fe–Ti oxides of the Lac des

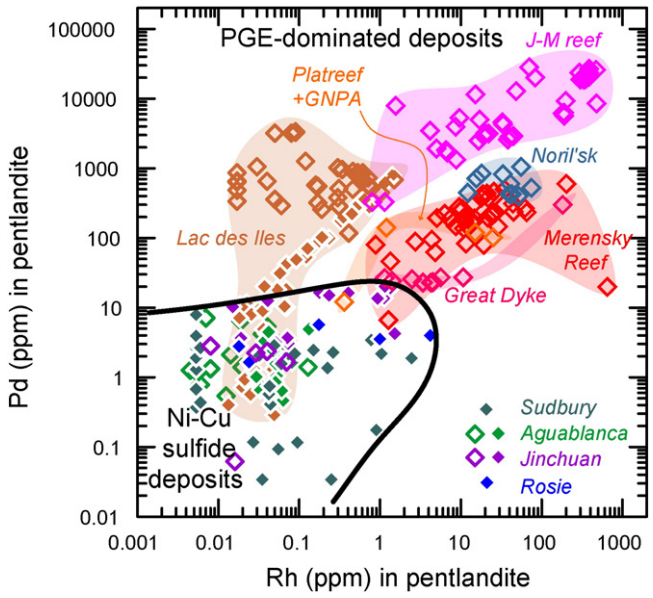

Fig. 20. Binary diagram of Pd in pentlandite versus Rh in pentlandite. Note that pentlandites from PGE-dominated deposits can be discriminated from pentlandites from Ni–Cu sulfide deposits on the basis of their Pd and Rh concentrations. The data sources are: Holwell and McDonald (2007), Godel et al. (2007), and Smith et al. (2014) for the Bushveld Complex (Merensky Reef, Platreef and GNPA member), Barnes et al. (2008) and Oberthür et al. (1997) for the Great Dyke, Godel and Barnes (2008) for the J–M Reef of the Stillwater Complex, Barnes et al. (2006) for Noril'sk, Djon and Barnes (2012) and this study for Lac des Iles (open diamonds = disseminated ore; closed diamonds = sulfide-rich pods), Dare et al. (2011) for Sudbury, Piña et al. (2012) for Aguablanca (open green diamonds = disseminated ore; closed green diamonds = semi-massive ore), Godel et al. (2012) for Rosie Nickel Prospect (blue diamonds), and Chen et al. (2014) for Jinchuan (open purple diamonds = disseminated ore; closed purple diamonds = massive and semi-massive ore).

Iles sulfide-rich pods and infer processes that influence this distribution. Our findings are summarized as follows:

1. The sulfide mineral compositions of the Lac des Iles sulfide-rich pods exhibit similarities to sulfide minerals derived from evolved magmas (e.g., Sudbury and Aguablanca) and do not resemble sulfide minerals derived from primitive magmas. For example, Lac des Iles sulfides are IPGE-poor. Hence we suggest that Lac des Iles parental magmas, at the time of ore formation, were evolved, most likely of andesitic composition. Thus, the trace element signature of sulfides could be used as a petrogenetic indicator in poorly understood settings.
2. The distribution of PGE and chalcophile elements among the primary BMS at Lac des Iles was initially governed by their partitioning behavior during the crystal fractionation of MSS. The similar trace element signature of sulfide minerals from the massive pods and the disseminated mineralization suggests a common origin for both types of mineralization.
3. Magnetite crystallized after the sulfides and recorded the signature of crystal fractionation of sulfide liquids. Magnetite co-crystallized with ilmenite, and Fe–Ti oxides were formed either directly from sulfide liquids or by reaction of oxygen with silicate liquids as it diffused out of the sulfide liquids.
4. Pyrrhotite and pentlandite contain significant amounts of Co and IPGE. The pentlandite also hosts significant amounts of Rh and Pd. These observations suggest that elements that were initially concentrated in MSS have been redistributed by exsolution of pyrrhotite and pentlandite. Rhenium and Mo that are compatible elements in MSS are present as discrete phases. These phases may have exsolved from MSS, coeval with pyrrhotite and pentlandite.
5. Chalcopyrite is enriched in Ag, Cd, and Zn relative to pyrrhotite and pentlandite, but is not enriched in Pd, Pt, Au, and semi-metals (Te, Sb, Bi and As), which suggests that chalcopyrite has exsolved from ISS. Platinum, Au, and semi-metals are not significantly present in BMS and are suspected to be mainly present as discrete PGM and electrum formed by crystallization of late fractionated liquids.
6. The heterogeneous distributions of Ag, Bi, and Pb within the pentlandite and some of the pyrrhotite suggest that the sulfide-rich pods have undergone some deformation-induced metal redistribution. However, the distribution of the PGE has not been influenced by this process.
7. The Pd and Rh concentrations of pentlandites from PGE-dominated deposits strongly differ from those of pentlandites from Ni–Cu sulfide deposits. Therefore, the use of the plot Pd versus Rh in pentlandite has a strong potential in exploration to discriminate between the possible sources of pentlandite in glaciated terrains.

Acknowledgments

This study was completed by the first author as part of his PhD research project at UQAC. We are grateful to North American Palladium for providing financial support to the Sarah-Jane Barnes' Canada Research Chair in Magmatic Ore Deposits, for allowing access to the mine property and publication of this paper, and for hiring the first author as an exploration geologist during field seasons. We would also like to thank the entire North American Palladium Exploration Team for technical support in the field over the years. Dany Savard and Sadia Mehdi are thanked for their assistance with the LA–ICP-MS facilities at LabMaTer, UQAC. This study largely benefited from intellectual input from Philippe Pagé and Ed Sawyer of UQAC, Sarah Dare of University of Ottawa, and Lionnel Djon, Arnaud Tchalikian, and Skylar Schmidt of North American Palladium. Finally, this manuscript benefited from thorough and insightful reviews by Rubén Piña, an anonymous reviewer, and associate editor Agustín Martín-Izard. Agustín Martín-Izard and Benedetto De Vivo are also thanked for their careful editorial handling.

Appendix A. Supplementary data

Supplementary data to this article can be found online at http://dx.doi.org/10.1016/j.gexplo.2016.04.005.

References

Averill, S., 2001. The application of heavy indicator mineralogy in mineral exploration, with emphasis on base metal indicators in glaciated metamorphic and plutonic terrain. In: McClenaghan, M.B., Bobrowsky, P.T., Hall, G.E.M., Cook, S.J. (Eds.), Drift Exploration in Glaciated Terrain. Geological Society, London, Special Publications Vol. 185, pp. 69–81.

Averill, S.A., 2011. Viable indicator minerals in surficial sediments for two major base metal deposit types: Ni–Cu–PGE and porphyry Cu. Geochem. Explor. Environ. Anal. 11, 279–291.

Barnes, S.-J., Gomwe, T.S., 2010. Composition of the Lac des Iles magma and implications for the origin of the ore. 10th International Platinum Symposium, Program Abstracts, Ontario Geological Survey, Miscellaneous Release, Data 269 (Extended Abstract).

Barnes, S.-J., Gomwe, T.S., 2011. The Pd deposits of the Lac des Iles Complex, Northwestern Ontario. Rev. Econ. Geol. 17, 351–370.

Barnes, S.-J., Lightfoot, P.C., 2005. Formation of magmatic nickel sulfide ore deposits and processes affecting their copper and platinum group element contents. Econ. Geol. 100th Anniversary Volume, 179–213.

Barnes, S.-J., Naldrett, A.J., Gorton, M.P., 1985. The origin of the fractionation of platinum-group elements in terrestrial magmas. Chem. Geol. 53, 303–323.

Barnes, S.-J., Makovicky, E., Karup-Moller, S., Makovicky, M., Rose-Hansen, J., 1997. Partition coefficients for Ni, Cu, Pd, Pt, Rh and Ir between monosulfide solid solution and sulfide liquid and the implications for the formation of compositionally zoned Ni–Cu sulfide bodies by fractional crystallization of sulfide liquid. Can. J. Earth Sci. 34, 366–374.

Barnes, S.-J., Cox, R.A., Zientek, M.L., 2006. Platinum-group element, gold, silver and base metal distribution in compositionally zoned sulfide droplets from the Medvezky Creek Mine, Noril'sk, Russia. Contrib. Mineral. Petrol. 152, 187–200.

Barnes, S.-J., Prichard, H.M., Cox, R.A., Fisher, P.C., Godel, B., 2008. The location of the chalcophile and siderophile elements in platinum group element ore deposits (a textural, microbeam and whole rock geochemical study): implications for the formation of the deposits. Chem. Geol. 248, 295–317.

Boudreau, A., Djon, L., Tchalikian, A., Corkery, J., 2014. The Lac des Iles palladium deposit, Ontario, Canada. Part I. The effect of variable alteration on the Offset Zone. Mineral. Deposita 49, 625–654.
Boutroy, E., Dare, S.A.S., Beaudoin, G., Barnes, S.-J., Lightfoot, P.C., 2014. Magnetite composition in Ni–Cu–PGE worldwide: application to mineral exploration. J. Geochem. Explor. 145, 64–81.
Brenan, J.M., 2008. Re–Os fractionation by sulfide melt–silicate melt partitioning: a new spin. Chem. Geol. 248, 140–165.
Brügmann, G.E., Reischrnann, T., Naldrett, A.J., Sutcliffe, R.H., 1997. Roots of an Archean volcanic arc complex; the Lac des Iles area in Ontario, Canada. Precambrian Res. 81, 223–239.
Buddington, A.F., Lindsley, D.H., 1964. Iron–titanium oxide minerals and synthetic equivalents. J. Petrol. 5, 310–357.
Cabri, L.J., 1973. New data on phase relations in the Cu–Fe–S system. Econ. Geol. 68, 443–454.
Campbell, I.H., Naldrett, A.J., 1979. The influence of silicate: sulphide ratios on the geochemistry of magmatic sulphides. Econ. Geol. 74, 1503–1506.
Chen, L.-M., Song, X.-Y., Danyushevsky, L.V., Wang, Y.-S., Tian, Y.-L., Xiao, J.-F., 2014. A laser ablation ICP-MS study of platinum-group and chalcophile elements in base metal sulfide minerals of the Jinchuan Ni–Cu sulfide deposit, NW China. Ore Geol. Rev. 65, 955–967.
Craig, J.R., 1973. Pyrite–pentlandite assemblages and other low temperature relations in the Fe–Ni–S systems. Am. J. Sci. 273A, 496–510.
Dare, S.A.S., Barnes, S.-J., Prichard, H.M., 2010. The distribution of platinum group elements and other chalcophile elements among sulfides from the Creighton Ni–Cu–PGE sulfide deposit, Sudbury, Canada, and the origin of Pd in pentlandite. Mineral. Deposita 45, 765–793.
Dare, S.A.S., Barnes, S.-J., Prichard, H.M., Fisher, P.C., 2011. Chalcophile and platinum-group element (PGE) concentrations in the sulfide minerals from the McCreedy East deposit, Sudbury, Canada, and the origin of PGE in pyrite. Mineral. Deposita 46, 381–407.
Dare, S.A.S., Barnes, S.-J., Beaudoin, G., 2012. Variation in trace element content of magnetite crystallized from a fractionating sulfide liquid, Sudbury, Canada: implications for provenance discrimination. Geochim. Cosmochim. Acta 88, 27–50.
Dare, S.A.S., Barnes, S.-J., Prichard, H.M., Fisher, P.C., 2014a. Mineralogy and geochemistry of Cu-rich ores from the McCreedy East Ni–Cu–PGE Deposit (Sudbury, Canada): Implications for the behavior of platinum group and chalcophile elements at the end of crystallization of a sulfide liquid. Econ. Geol. 109, 343–366.
Dare, S.A.S., Barnes, S.-J., Beaudoin, G., Méric, J., Boutroy, E., Potvin-Doucet, C., 2014b. Trace elements in magnetite as petrogenetic indicators. Mineral. Deposita 49, 785–796.
Djon, M.L.N., Barnes, S.-J., 2012. Changes in sulphides and platinum-group minerals with the degree of alteration in the Roby, Twilight, and High Grade Zones of the Lac des Iles Complex, Ontario, Canada. Mineral. Deposita 47, 875–896.
Dupuis, C., Beaudoin, G., 2011. Discriminant diagrams for iron oxide trace element fingerprinting of mineral deposit types. Mineral. Deposita 46, 319–335.
Duran, C.J., Barnes, S.-J., Corkery, J.T., 2015. Chalcophile and platinum-group element distribution in pyrites from the sulfide-rich pods of the Lac des Iles Pd deposits, Western Ontario, Canada: Implications for post-cumulus re-equilibration of the ore and the use of pyrite compositions in exploration. J. Geochem. Explor. 158, 223–242.
Duran, C.J., Barnes, S.-J., Corkery, J.T., 2016. Geology, petrography, geochemistry, and genesis of sulfide-rich pods in the Lac des Iles palladium deposits, western Ontario, Canada. Mineral. Deposita 51, 509–532. http://dx.doi.org/10.1007/s00126-015-0622-z.
Dutrizac, J.E., 1976. Reactions in cubanite and chalcopyrite. Can. Mineral. 14, 172–181.
Fonseca, R.O.C., Campbell, A.H., O'Neill, H.S.C., Fitzgerald, J.D., 2008. Oxygen solubility and speciation in sulphide-rich mattes. Geochim. Cosmochim. Acta 72, 2619–2635.
Godel, B., Barnes, S.-J., 2008. Platinum-group elements in sulfide minerals and the whole rocks of the J–M Reef (Stillwater Complex): implication for the formation of the reef. Chem. Geol. 248, 272–294.
Godel, B., Barnes, S.-J., Maier, W.M., 2007. Platinum-group elements in sulfide minerals, platinum-group minerals, and whole-rocks of the Merensky Reef (Bushveld Complex, South Africa): Implications for the formation of the reef. J. Petrol. 48, 1569–1604.
Godel, B., González-Álvarez, I., Barnes, S.J., Barnes, S.-J., Parker, P., Day, J., 2012. Sulfides and sulfarsenides from the Rosie Nickel Prospect, Duketon greenstone belt, Western Australia. Econ. Geol. 107, 275–294.
Golightly, P.J., 1994. The Sudbury igneous complex as an impact melt: evolution and ore genesis. In: Lightfoot, P.C., Naldrett, A.J. (Eds.), Proceedings of the Sudbury-Noril'sk Symposium. Ontario Ministry of Northern Development and Mines, Ontario Geological Survey (105–118 pp.).
Gupta, V.K., Sutcliffe, R.H., 1990. Mafic–ultramafic intrusives and their gravity field: Lac des Iles area, northern Ontario. Geol. Soc. Am. Bull. 102, 1471–1483.
Hanley, J.J., Gladney, E.R., 2011. The presence of carbonic-dominant volatiles during the crystallization of sulfide-bearing mafic pegmatites in the North Roby Zone, Lac des Iles Complex. Ontario. Econ. Geol. 106, 33–54.
Helmy, H.M., Ballhaus, C., Wohlgemuth-Ueberwasser, C., Fonseca, R.O.C., Laurenz, V., 2010. Partitioning of Se, As, Sb, Te and Bi between monosulfide solid solution and sulfide melt — application to magmatic sulfide deposits. Geochim. Cosmochim. Acta 74, 6174–6179.
Hinchey, J.G., Hattori, K.H., 2005. Magmatic mineralization and hydrothermal enrichment of the High Grade Zone at the Lac des Iles palladium mine, northern Ontario, Canada. Mineral. Deposita 40, 13–23.
Hinchey, J.G., Hattori, K.H., Lavigne, M.J., 2005. Geology, petrology, and controls on PGE mineralization of the southern Roby and Twilight zones, Lac des Iles mine, Canada. Econ. Geol. 100, 43–61.
Holwell, D.A., McDonald, I., 2007. Distributions of platinum-group elements in the Platreef at Overysel, northern Busveld Complex: a combined PGM and LA–ICP-MS study. Contrib. Mineral. Petrol. 154, 171–190.
Huminicki, M.A.E., Sylvester, P.J., Cabri, L.J., Lesher, M.C., Tubrett, M., 2005. Quantitative mass balance of platinum-group elements in the Kelly Lake Ni–Cu–PGE deposit, Copper Cliff Offset, Sudbury. Econ. Geol. 100, 1631–1646.
Hutchinson, D., McDonald, I., 2008. Laser ablation ICP-MS study of platinum-group elements in sulphides from the Platreef at Turfspruit, northern limb of the Bushveld Complex, South Africa. Mineral. Deposita 43, 695–711.
Kelly, D.P., Vaughan, D.J., 1983. Pyrrhotine-pentlandite ore textures: a mechanistic approach. Mineral. Mag. 47, 453–463.
Kress, V., Greene, L.E., Ortiz, M.D., Mioduszewski, L., 2008. Thermochemistry of sulfide liquids IV: density measurements and the thermodynamics of O–S–Fe–Ni–Cu liquids a low to moderate pressures. Contrib. Mineral. Petrol. 156, 785–797.
Lavigne, M.J., Michaud, M.J., 2001. Geology of North American Palladium Ltd'.s Roby Zone Deposit, Lac des Iles. Explor. Min. Geol. 10, 1–17.
Lesher, C.M., Keays, R.R., 2002. Komatiite-associated Ni–Cu–(PGE) deposits: mineralogy, geochemistry, and genesis. In: Cabri, L.J. (Ed.), The Geology, Geochemistry, Mineralogy, and Mineral Beneficiation of the Platinum-Group Elements. Canadian Institute of Mining, Metallurgy, and Petroleum, Spec Vol 54, pp. 579–617.
Li, Y., Audétat, A., 2012. Partitioning of V, Mn, Co, Ni, Cu, Zn, As, Mo, Ag, Sn, Sb, W, Au, Pb, and Bi between sulfide phases and hydrous basanite melt at upper mantle conditions. Earth Planet. Sci. Lett. 355–356, 327–340.
Li, C., Barnes, S.-J., Makovicky, E., Rose-Hansen, J., Makovicky, M., 1996. Partitioning of Ni, Cu, Ir, Rh, Pt and Pd between monosulfide solid solution and sulfide liquid: effects of composition and temperature. Geochim. Cosmochim. Acta 60, 1231–1238.
Liu, Y., Brenan, J., 2015. Partitioning of platinum-group elements (PGE) and chalcogens (Se, Te, As, Sb, Bi) between monosulfide-solid solution (MSS), intermediate solid solution (ISS) and sulfide liquid at controlled fO_2–fS_2 conditions. Geochim. Cosmochim. Acta 159, 139–161.
Lyubetskaya, T., Korenaga, J., 2007. Chemical composition of Earth's primitive mantle and its variance: 1. Method and results. J. Geophys. Res. 112, B03211. http://dx.doi.org/10.1029/2005JB004223.
McClenaghan, M.B., 2005. Indicator mineral methods in mineral exploration. Geochem. Explor. Environ. Anal. 5, 233–245.
McClenaghan, M.B., Cabri, L.J., 2011. Review of gold and platinum group element (PGE) indicator minerals methods for surficial sediment sampling. Geochem. Explor. Environ. Anal. 11, 251–263.
McClenaghan, M.B., Averill, S.A., Kjarsgaard, I.M., Layton-Matthews, D., Matile, G., 2011. Indicator mineral signatures of magmatic Ni–Cu deposits, Thompson Nickel Belt, central Canada. In: McClenaghan, B., Peuraniemi, V., Lehtonen, M. (Eds.), Indicator Mineral Methods in Mineral ExplorationWorkshop in the 25th International Applied Geochemistry Symposium 2011, 22–26 August 2011 Rovaniemi. Finland, Vuorimiesyhdistys, pp. B92–B94 (72 pp.).
McClenaghan, M.B., Plouffe, A., Layton-Matthews, D., 2014. Application of indicator mineral methods to mineral exploration. Geol. Surv. Can. Open File 7553 (74 pp.).
Méric, J., 2011. Caractérisation géochimiques des magnétites de la zone critique de l'intrusion magmatique de Sept-Iles (Québec, Canada) et intégration a une base de données utilisant la signature géochimique des oxydes de fer comme outil d'exploration. Université du Québec à Chicoutimi - Université Montpellier 2 (Honors Thesis). (48 pp.).
Misson, P.-J., Barnes, S.-J., Pagé, P., 2013. What happened during the metamorphism of Ni–Cu–PGE deposit: the example of the Delta deposit (Raglan area, Northern Quebec). GAC-MAC Joint Annual Meeting, Abstract Volume 37, p. 192 (abstract).
Mota-e-Silva, J., Prichard, H.M., Ferreira Filho, C.F., Fisher, P.C., McDonald, I., 2015. Platinum-group minerals in the Limoeiro Ni–Cu–(PGE) sulfide deposit, Brazil: the effect of magmatic and upper amphibolite to granulite metamorphic processes on PGM formation. Mineral. Deposita http://dx.doi.org/10.1007/s00126-015-0585-0.
Mungall, J.E., Andrews, D.R.A., Cabri, L.J., Sylvester, P., Tubrett, M., 2005. Partitioning of Cu, Ni, Au, and platinum-group elements between monosulfide solid solution and sulfide melt under controlled oxygen and sulfur fugacities. Geochim. Cosmochim. Acta 69, 4349–4360.
Nadoll, P., Angerer, T., Mauk, J.L., French, D., Walshe, J., 2014. The chemistry of hydrothermal magnetite: a review. Ore Geol. Rev. 61, 1–32.
Naldrett, A.J., 1969. A portion of the system Fe–S–O between 900 and 1080 °C and its application to sulfide ore magmas. J. Petrol. 10, 171–201.
Naldrett, A.J., 2004. Magmatic Sulfide Deposits: Geology, Geochemistry and Exploration. Springer, Berlin (727 pp.).
Naldrett, A.J., Craig, J.R., Kullerud, G., 1967. The central portion of the Fe–Ni–S system and its bearing on pentlandite exsolution in iron-nickel sulfide ores. Econ. Geol. 62, 826–847.
Néron, A., 2012. Caractérisation géochimiques des oxydes de Fe–Ti dans un dépôt de Fe–Ti–P associe à la suite anorthositique de Lac Saint Jean, Québec, Canada (secteur Lac à Paul) et intégration des données du secteur Lac à La Mine. Université du Québec à Chicoutimi (Honors Thesis). (39 pp.).
Oberthür, T., Cabri, L.J., Weiser, T.W., McMahon, G., Müller, P., 1997. Pt, Pd and other trace elements in sulfides of the Main Sulfide Zone, Great Dyke, Zimbabwe: a reconnaissance study. Can. Mineral. 35, 597–609.
Osbahr, I., Klemd, R., Oberthür, T., Brätz, H., Schouwstra, R., 2013. Platinum-group element distribution in base-metal sulfides of the Merensky Reef from the eastern and western Bushveld Complex, South Africa. Mineral. Deposita 48, 211–232.
Osbahr, I., Oberthür, T., Klemd, R., Josties, A., 2014. Platinum-group element distribution in base-metal sulfides of the UG2 chromitite, Bushveld Complex, South Africa — a reconnaissance study. Mineral. Deposita 49, 655–665.
Paton, C., Hellstrom, J., Paul, B., Woodhead, J., Hergt, J., 2011. Iolite: freeware for the visualisation and processing of mass spectrometric data. J. Anal. At. Spectrom. 26, 2508–2518.

Piña, R., Gervilla, F., Ortega, L., Lunar, R., 2008. Mineralogy and geochemistry of platinum-group elements in the Aguablanca Ni–Cu deposit (SW Spain). Mineral. Petrol. 92, 259–282.
Piña, R., Gervilla, F., Barnes, S.-J., Ortega, L., Lunar, R., 2012. Distribution of platinum-group and chalcophile elements in the Aguablanca Ni–Cu sulfide deposit (SW Spain): evidence from a LA–ICP-MS study. Chem. Geol. 302–303, 61–75.
Piña, R., Gervilla, F., Barnes, S.-J., Ortega, L., Lunar, R., 2013. Platinum-group elements-bearing pyrite from the Aguablanca Ni–Cu sulphide deposit (SW Spain): a LA–ICP-MS study. Eur. J. Mineral. 25, 241–252.
Pokrovski, G.S., Borisova, A.Y., Bychkov, A.Y., 2013. Speciation and transport of metals and metalloids in geological vapors. Rev. Mineral. Geochem. 76, 165–218.
Rankin, L.R., 2013. Structural controls on emplacement and deformation of PGE-mineralised mafic–ultramafic intrusions — LDI district, NW Ontario. North American Palladium Technical Report (115 pp.).
Rudnick, R.L., Gao, S., 2003. Composition of the continental crust. In: Holland, H.D., Turekian, K.K. (Eds.), Treatise on Geochemistry Vol. 3. Elsevier, Oxford (1–64 pp.).
Schisa, P., Boudreau, A., Djon, L., Tchalikian, A., Corkery, J., 2015. The Lac des Iles palladium deposit, Ontario, Canada. Part II. Halogen variations in apatite. Mineral. Deposita 50, 339–355.
Smith, J.W., Holwell, D.A., McDonald, I., 2014. Precious and base metal geochemistry and mineralogy of the Grasvally Norite-Pyroxenite-Anorthosite (GNPA) member, northern Bushveld Complex, South Africa: implications for a multistage emplacement. Mineral. Deposita 49, 667–692.
Somarin, A.K., Kissin, S.A., Heerema, D.D., Bihari, D.J., 2009. Hydrothermal alteration, fluid inclusion and stable isotope studies of the north Roby Zone, Lac des Iles PGE mine, Ontario, Canada. Resour. Geol. 59, 107–120.
Stone, D., Lavigne, M.J., Schnieders, B., Scott, J., Wagner, D., 2003. Regional geology of the Lac des Iles Area. *Ontario* Geological Survey. Open File Rep. 6120 (15–1) (15-25 pp.).
Sutcliffe, R.H., Sweeny, J.M., Edgar, A.D., 1989. The Lac des Iles Complex, Ontario: petrology and platinum-group-elements mineralization in an Archean mafic intrusion. Can. J. Earth Sci. 26, 1408–1427.
Talkington, R.W., Watkinson, D.H., 1984. Trends in the distribution of the precious metals in the Lac-Des-Iles Complex, Northwestern Ontario. Can. Mineral. 22, 125–136.
Tomkins, A.G., Rebryna, K.C., Weinberg, R.F., Schaefer, F., 2012. Magmatic sulfide formation by reduction of oxidized arc basalt. J. Petrol. 53, 1537–1567.
Vukmanovic, Z., Reddy, S.M., Godel, B., Barnes, S.J., Fiorentini, M.L., Barnes, S.-J., Kilburn, M.R., 2014. Relationship between microstructures and grain-scale trace element distribution in komatiite-hosted magmatic sulphide ores. Lithos 302–303, 42–61.
Watkinson, D.H., Dunning, G.R., 1979. Geology and platinum-group mineralization, Lac des Iles complex, northwestern Ontario. Can. Mineral. 17, 453–462.